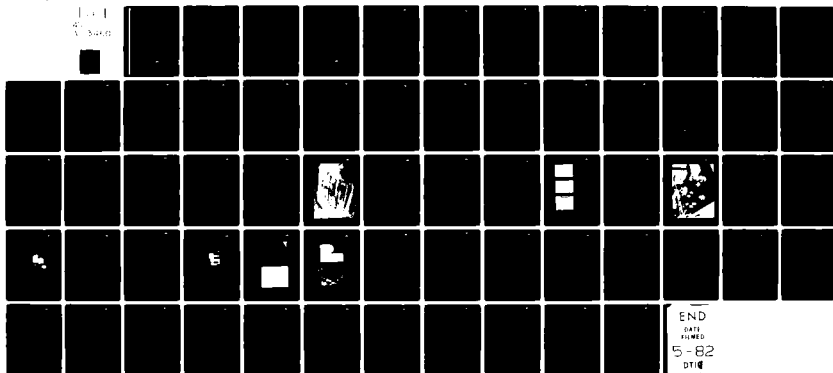


AD-A113 460

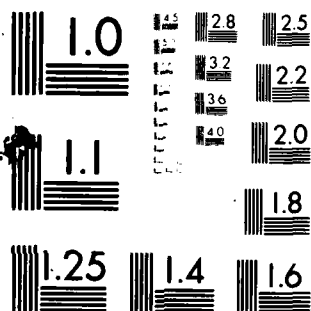
ROCKWELL INTERNATIONAL DOWNEY CA SATELLITE SYSTEMS DIV F/G 9/5  
SOLID-STATE MILLIMETER-WAVE SOURCE STUDY: A STUDY OF TWO NOVEL --ETC(U)  
SEP 81 J 500H00 DAAK70-79-C-0083  
C79-606.12/501 NL

UNCLASSIFIED

1-1  
1-2  
1-3



END  
DATE  
FILMED  
5-82  
DTIC



MICROCOPY RESOLUTION TEST CHART  
NATIONAL BUREAU OF STANDARDS-1963-A

②

AD A113460

C79-606.12/501

SOLID-STATE MILLIMETER-WAVE SOURCE STUDY:

A STUDY OF TWO NOVEL CONCEPTS FOR  
GENERATION OF CW MILLIMETER WAVES

SEPTEMBER 1981

PREPARED BY

JACK SOOHOO

DTIC FILE COPY

Space Operations/Integration &  
Satellite Systems Division



Rockwell  
International

12214 Lakewood Boulevard  
Downey, California 90241

DTIC  
ELECTE  
S APR 15 1982  
E

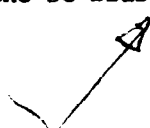
This document has been approved  
for public release and sale; its  
distribution is unlimited

82 04 15 010

REPORT DOCUMENTATION PAGE		READ INSTRUCTIONS BEFORE COMPLETING FORM
1. REPORT NUMBER	2. GOVT ACCESSION NO.	3. RECIPIENT'S CATALOG NUMBER
	AD-A113 460	
4. TITLE (and Subtitle) Solid State Millimeter-Wave Source Study: A Study of two Novel Concepts for Generation of CW Millimeter Waves		5. TYPE OF REPORT & PERIOD COVERED Final Report July 1979 - October 1981
		6. PERFORMING ORG. REPORT NUMBER
7. AUTHOR(s) Jack Soohoo		8. CONTRACT OR GRANT NUMBER(s) DAAK70-79-C-0043
9. PERFORMING ORGANIZATION NAME AND ADDRESS Rockwell International 12214 Lakewood Boulevard Downey, CA 90241		10. PROGRAM ELEMENT, PROJECT, TASK AREA & WORK UNIT NUMBERS 61102A 1L161102A31B LØ 004 CJ
11. CONTROLLING OFFICE NAME AND ADDRESS Night Vision and Electro-Optics Laboratory ATTN: DELNV-L Ft. Belvoir, VA 22060		12. REPORT DATE September 1981
		13. NUMBER OF PAGES 56
14. MONITORING AGENCY NAME & ADDRESS (if different from Controlling Office)		15. SECURITY CLASS. (of this report)  UNCLASSIFIED
		15a. DECLASSIFICATION/DOWNGRADING SCHEDULE
16. DISTRIBUTION STATEMENT (of this Report)  Approved for public release; distribution unlimited.		
17. DISTRIBUTION STATEMENT (of the abstract entered in Block 20, if different from Report)		
18. SUPPLEMENTARY NOTES		
19. KEY WORDS (Continue on reverse side if necessary and identify by block number)  Millimeter Wave Source, travelling wave, solid state source, laser modulation, ridge waveguide, distributed source, IMPATT source		
20. ABSTRACT (Continue on reverse side if necessary and identify by block number) Two novel device concepts for generating CW millimeter waves with output power in the multi-watt range were investigated. The first concept involves the utilization of modulated laser radiation to induce in a distributed Schottky diode structure a travelling-wave current which, in turn, synchronously excites the dominant mode of a waveguide structure to generate millimeter power. The induced travelling-wave current is directly proportional to the laser modulation generated by the interference of two overlapping laser beams of millimeter beat frequency. Experimentally, we have thus far demonstrated this concept of		

millimeter wave generation using a point-like HgCdTe diode/waveguide structure.

The second concept involves the use of a distributed IMPATT diode/waveguide structure. This structure is battery-operated and requires no optical excitation, simply an elongated Read-type diode in the gap of a specially designed ridgeguide. In this structure, the field-current interaction is very strong, resulting in a growing travelling wave which extracts energy from the DC bias.



C79-606.12/501

SOLID-STATE MILLIMETER-WAVE SOURCE STUDY:

A STUDY OF TWO NOVEL CONCEPTS FOR  
GENERATION OF CW MILLIMETER WAVES

SEPTEMBER 1981

PREPARED BY

JACK SOOHOO

Space Operations/Integration &  
Satellite Systems Division



Rockwell  
International

12214 Lakewood Boulevard  
Downey, California 90241

Accession For	
NTIS CR&I	<input checked="checked" type="checkbox"/>
DTIC TAB	<input type="checkbox"/>
Unannounced	<input type="checkbox"/>
Justification	
By	
Distribution/	
Availability Codes	
Dist	Avail and/or Special
A	





## FOREWORD

This final report is submitted in accordance with Contract DAAK70-79-C0043, "Millimeter Source Study." It summarizes the results of a study to investigate two novel solid-state millimeter-wave sources.

The program was sponsored by the Night Vision and Electro-Optics Laboratory, U. S. Army Mobility Equipment and Research Command, Fort Belvoir, Va. J. E. Miller of that laboratory was the program monitor.

C. L. Hayes and S. K. Yao served as the program manager from July 1979 to Oct. 1979 and from Oct. 1979 to June 1980, respectively; J. SooHoo served as the principal investigator from July 1979 to Oct. 1981, the duration of the program, and as the program manager from June 1980 to Oct. 1981.

In addition to J. E. Miller and R. R. Shurtz, II of the Night Vision and Electro-Optics Laboratory, the major contributors to this program are the following people (in alphabetical order):

R. A. Gudmundsen  
C. L. Hayes  
E. H. Huffman  
F. Ryan  
J. SooHoo  
Y. Taur  
P. Wang  
S. K. Yao

## TABLE OF CONTENTS

Chapter		Page
1.0	INTRODUCTION. . . . .	1
2.0	FORMULATION AND CALCULATION OF THE LASER-INDUCED TRAVELING-WAVE SOURCE CONCEPT . . . . .	6
3.0	EXPERIMENTS OF THE LASER-INDUCED CONCEPTS . . . . .	22
4.0	TRAVELLING-WAVE IMPATT MODE IN A RIDGEGUIDE CONFIGURATION.	
5.0	CONCLUSIONS . . . . .	
	APPENDIX A. TRANSMISSION LINE MODEL. . . . .	42
	APPENDIX B. WAVEGUIDE MODEL . . . . .	48
	APPENDIX C. WAVEVECTOR ERROR DUE TO MISALIGNMENT ERRORS .	52
6.0	REFERENCES . . . . .	55



## ILLUSTRATIONS

Figure		Page
1	Simplified Illustration of the Laser-Induced Travelling-Wave Device. . . . .	3
2	Functional Block Diagram of the Travelling-Wave Device. . . . .	4
3	Cross Sectional Views of Two Low-Impedance and Wideband Waveguide Configurations (not to scale) . . . . .	15
4	Single-Ridge Configuration (not to scale) . . . . .	16
5	Millimeter Power Along the 5 mm Long HgCdTe Layer in Gap of Single-Ridge Guide at 77° with Impedance Matched: Upper Curve is for the Phase-Match Case, While Lower Curve Shows Effect of Phase Mismatch Due to Laser Misalignment. . . . .	19
6	Millimeter Power P Along the 5 mm HgCdTe Active Retension in Gap of Single-Ridge Guide at 77° with Impedance and Phase Matched (see Table 4 for the Other Parameter Values) . . . . .	20
7	Photograph of the Waveguide CO Lasers . . . . .	23
8	Top and Cross Sectional View of the Heterostructure n <sup>+</sup> /p HgCdTe Photodiode (The thickness of the epitaxial layer is n not drawn to scale.) . . . . .	24
9	Diode Chip Mounted in a Reduced-Height mm-Wave Waveguide (The longer dimension of the waveguide is 2.54 mm.) . . . . .	26
10	Diode I-V Curves and Characteristics. . . . .	27
11	Photograph of Millimeter Experimental Setup . . . . .	29
12	Finline Guide Drawing (not to scale) . . . . .	31
13	Photograph of Distributed Diode/Waveguide Configuration (This design is for operation at 100 GHz.) . . . . .	32
14	Quartz (SiO <sub>2</sub> ) Holder and HgCdTe/CdTe Strip Diode. . . . .	33
15	Amplitude Reflection Coefficient (r) Vs. Normalized Taper Length ( $2/\lambda_g$ ) (Finline). . . . .	34
16	Photograph of a Broken Diode/Finline Structure . . . . .	35
17	Photographs of Typical HgCdTe Sample Surface (see reference scale) . . . . .	36
18	Photographs of Typical HgCdTe Sample. . . . .	37
A-1	Diagram of an Arbitrarily Terminated Transmission Line. . . . .	39
C-1	Diagram of Wave Vector Mismatch Due to Laser Misalignment . . . . .	49



TABLES

Table		Page
1	Partial List of CO Laser Transitions with Beat Frequencies Near 240 GHz . . . . .	9
2	Partial List of CO Laser Transitions with Beat Frequencies Near 95 GHz . . . . .	9
3	Parameter Values of HgCdTe at 77°K . . . . .	10
4	Partial List of Parameter Values used in the Calculations .	18

## ABSTRACT

We have investigated two novel device concepts for generating CW millimeter waves with output power in the multi-watt range. Implementation of the concepts appears feasible with existing solid state technologies.

The first concept involves the utilization of modulated laser radiation to induce in a distributed Schottky diode structure a travelling-wave current which, in turn, synchronously excites the dominant mode of a waveguide structure to generate millimeter power. The induced travelling-wave current is directly proportional to the laser modulation generated by the interference of two overlapping laser beams of millimeter beat frequency. Detailed analysis indicates that the device has both high-output and frequency-tunable characteristics. Experimentally, we have thus far demonstrated this concept of millimeter wave generation using a point-like HgCdTe diode/waveguide structure.

The second concept involves the use of a distributed IMPATT diode/waveguide structure. This structure is battery-operated and requires no optical excitation, simply an elongated Read-type diode in the gap of a specially designed ridgeguide. As in point-like IMPATT diodes, the current which generates the millimeter power is induced by the avalanche effect. In this particular structure, however, the field-current interaction is very strong, resulting in a growing travelling wave which extracts energy from the DC bias. Although preliminary analytical results for this structure using Si and GaAs parameter values appear very promising, a more detailed study should be performed.



## 1.0 INTRODUCTION

### A. BACKGROUND

The advantages of millimeter waves in many applications have renewed significant interest in the exploitation of that portion of the electromagnetic spectrum. In comparison with visible light and infrared waves, millimeter waves penetrate smoke, dust, fog and clouds. As compared with centi-meter microwaves, millimeter waves offer smaller-size systems and increased spatial and temporal resolutions. These advantages of millimeter waves over electro-optics and microwaves are important for many military applications, such as short-range radar, missile seeker, imaging and covert communications.

As for the state-of-the-art CW millimeter wave sources, gyrotron and tube-type systems are capable of generating very high output power, (in the kilowatt range) but these systems are impractical for most military applications because of their large sizes. Compact solid-state, transit-time devices such as IMPATT diodes can produce about a watt of CW power at 100 GHz, but their output power drops rapidly with increasing frequency, to only tens of milliwatts near 200 GHz. Although various power-combine techniques (at both device and circuit levels) have been used to coherently combine the output of individual IMPATT diodes, these techniques have not been satisfactory, mainly due to the rapid increase of insertion and path losses as the number of diodes increases. At present a compact solid-state millimeter wave source capable of generating even a few watts of CW power is still unavailable. Such a device would have significant impact on military systems applications.

### B. SCOPE

This research is concerned with two novel concepts for generating high-power CW millimeter waves, both of which appear to be implementable with existing solid state technologies.

One of the concept involves the use of two laser beams to induce in a diode structure a CW photocurrent which, in turn, drives a wave guide structure to generate millimeter waves under phase-matching condition<sup>1,2</sup>.

B. SCOPE (Continued)

Since the inception of this idea, a great deal of analysis has been performed. We have found that most of the analysis may be applied to a broad class of devices, not necessarily limited to those excited by lasers or other optical means. For simplicity of implementation, in fact, it appears that certain types of all-semiconductor transit-time devices seem to have greater potential than the optical approach. The concept is simply illustrated in Figure 1. Here, the current source is a consequence of the laser-induced carriers within the depletion layer of a reverse-biased strip Schottky diode which, itself, is part of the millimeter wave structure. The diode is reverse biased to saturation so that the carriers are swept out of the depletion layer at their saturation velocity. These carriers are generated through the absorption of energy from the two interfering laser beams of millimeter beat frequency. Figure 2 is a functional block diagram of the device. The laser intensities,  $I_1$  and  $I_2$ , are approximately equal. With the RF frequency of the AO cell as reference, the detector output drives a feedback loop (not shown) which, in turn, controls and stabilizes the laser beat frequency, or the output millimeter frequency. The angle between the two laser beams, which determines the phase velocity of the excited millimeter energy, is controlled by the turn mirror. The device is potentially compact and light-weight, because the required laser energy for excitation may be provided by small sealed-off waveguide lasers.

The other concept involves the use of a distributed IMPATT diode/waveguide structure. This structure is battery-operated and requires no optical excitation, simply consisting of an elongated Read-type diode in the gap of a ridged waveguide. The elongated, layered diode is sandwiched between and metallurgically bonded to the guide ceiling and ridge. As in point-like IMPATT diodes, the current which generates the mm energy is induced by the avalanche effect. In this particular distributed structure, however, the field-current interaction is very strong, resulting in a growing traveling wave which extracts energy from the DC bias. Because of its relative simplicity in fabrication and in systems application, this structure is superior to the laser-induced or any other optically induced structures. The preliminary analytical results we have obtained for this structure using Si and GaAs parameter values appear very promising. We therefore suggest that the effort on the development of this distributed IMPATT structure be continued.

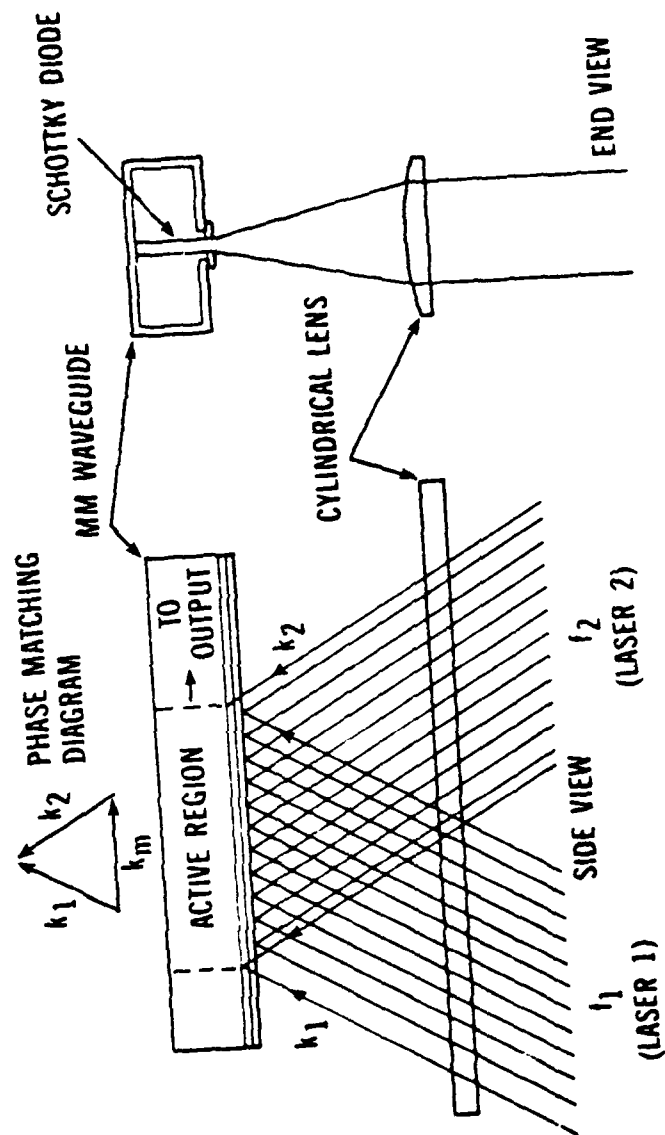


Figure 1. Simplified Illustration of the Laser-Induced Travelling-Wave Device

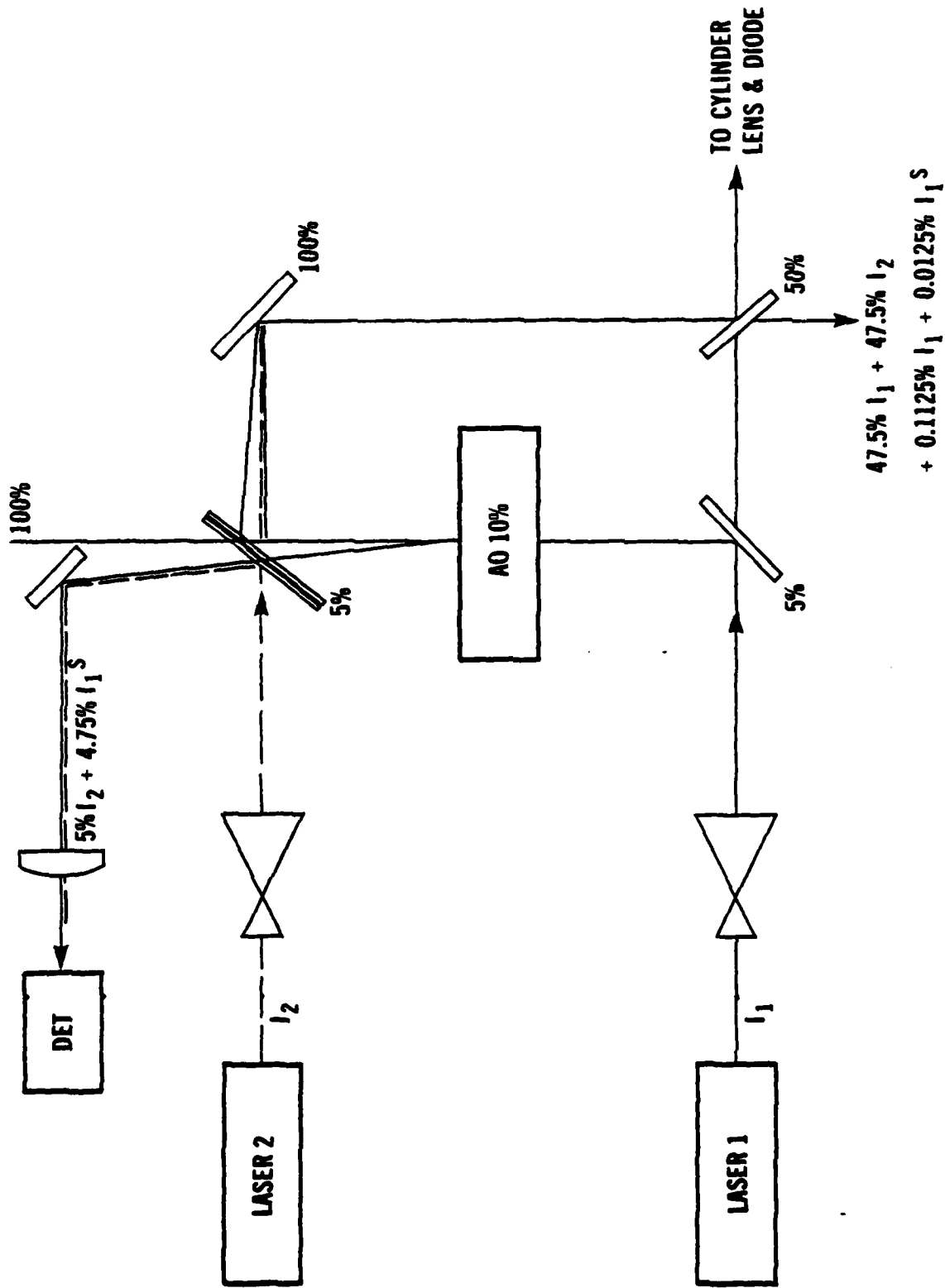


Figure 2. Functional Block Diagram of the Travelling-Wave Device



C. PRIMARY CONTRIBUTIONS

The primary contributions of this work are as follows:

1. Formulation and analysis of the laser-induced traveling-wave source concept.
2. Development of waveguide CO lasers and related components.
3. Development of laser-induced device configurations for CW millimeter-wave generation.
4. Experimental investigation of the laser-induced concept with epitaxial HgCdTe/CdTe as active medium.
5. Preliminary formulation and analysis of a simple and efficient distributed IMPATT structure for CW millimeter-wave generation.



## 2.0 FORMULATION AND CALCULATION OF THE LASER-INDUCED TRAVELING-WAVE SOURCE CONCEPT

When a propagating mode of a transmission line, or of a waveguide, is excited by a source distribution which propagates at the phase velocity of the mode fields, the traveling source and the mode fields are in phase synchronism. Under this condition energy from the source is coherently added to the mode fields. In other words, the interaction is phase-matched, and the energy of the fields "grows" as it propagates through the active region. A simple counterpart of this traveling-wave concept in the time domain would be that of a RLC circuit resonantly excited by a voltage source, or that of a harmonic oscillator which is driven by a force at resonance. In all these cases the response to the excitation is maximal.

### A. GENERAL CONSIDERATIONS

#### 1. Laser Power and Induced Current

The travelling-wave current in the depletion layer is induced by two overlapping laser beams. As depicted in Figure 1, the total electric field of the two lasers,  $E$ , in the depletion layer may be expressed as

$$E = E_0 \exp(i(\omega_1 t + k_1 z \sin \frac{\theta}{2})) + E_0 \exp(i(\omega_2 t - k_2 z \sin \frac{\theta}{2})) \quad (1)$$

where  $z$  is the direction along the waveguide axis,  $\theta$ , is the angle between the two beams of equal amplitude  $E_0$ ,  $\omega_i$  and  $k_i$ ,  $i = 1$  or  $2$ , are the laser frequencies and propagation constants, respectively. The effective laser intensity  $I$  illuminating the depletion layer is then of the form

$$I \sim |E|^2 = 2E_0^2 \left\{ 1 + \cos[(\omega_2 - \omega_1)t - (k_2 + k_1)z \sin \frac{\theta}{2}] \right\}, \quad (2)$$

which is a travelling-wave oscillating at the beat frequency  $\omega_2 - \omega_1$ . Thus, the induced current is also a travelling-wave since it is directly proportional to the laser intensity. While the DC term of the induced current contributes

to heat generation, the AC term is a current source of frequency  $\omega$  and of phase velocity  $V_p$  given by

$$\omega = \omega_2 - \omega_1$$

$$V_p = \frac{\omega_2 - \omega_1}{(k_2 + k_1) \sin \frac{\theta}{2}} \quad (3)$$

## 2. Material Absorptivity and Transit Time

To determine the effect of the material absorptivity,  $\alpha$ , we consider a strip Schottky diode structure consisting of an N-type layer sandwiched between a metal layer (M) and a N<sup>+</sup> layer substrate. In this MN<sup>+</sup> configuration the absorptivity of the N<sup>+</sup> substrate at the laser wavelength is made negligible compared with that of the active N layer of thickness W. Let  $\phi$  be the incident photon flux entering the depletion region at  $x = 0$ . Then the induced current density J in Amperes per unit area is <sup>3</sup>

$$J = -q\phi(1 - e^{-\alpha W}) \quad (4)$$

where q is the magnitude of the electron charge.

Assuming saturated drift velocity,  $V_s$ , the maximum density of electron-hole pairs, n, generated by an optical flux density,  $\phi$ , is given by

$$n = \frac{J}{qV_s} = \frac{\phi(1 - e^{-\alpha W})}{V_s} \quad (5)$$

Assuming an input power of 2 watts at a wavelength of 5.5  $\mu\text{m}$ , the maximum electron-hole density is  $1.05 \times 10^{14} \text{ cm}^{-3}$  in the depletion layer. The space charge field generated by this plasma is given by <sup>4</sup>

$$E = \frac{JW}{V_s \epsilon} = \frac{qnW}{\epsilon} \quad (6)$$

where  $\epsilon$  is the dielectric constant. For the photo-generated pair density calculated above, a depletion layer width of 1  $\mu\text{m}$ , and the material parameters

given in Table 3, the space charge field is calculated to be  $1.1 \times 10^3$  V/cm, which is well below the applied field ( $\sim 2 \times 10^4$  V/cm). Therefore, quasi-charge neutrality conditions leading to an ambipolar type of diffusion process are not relevant. Drift, not diffusion, dominates carrier flow through the depletion layer.

As the laser flux traverses the depletion layer, the contribution to the total current from individual electrons generated at a given point  $x$  along the path has a relative phase factor  $e^{-i\omega(W-x)/V_s}$ . For the worst case, in which we assume the electrons are uniformly generated within the entire depletion layer, the transit-time degradation factor  $B$  is simply obtained by averaging the phase factor as follows:

$$B = \frac{\int_0^W e^{-i\frac{\omega}{V_s}x} dx}{W} = \frac{\sin \omega\tau/2}{\omega\tau/2} \quad (7)$$

where  $\tau = W/V_s$ , the transit time across the depletion layer. Thus the induced millimeter wave current density taking into account the effect of both transit time and absorptivity is of the form:

$$J = J_0 (1 - e^{-\alpha W}) \frac{\sin \omega\tau/2}{\omega\tau/2} \cos \omega(t - z/V_p) \quad (8)$$

where  $J_0$  is in Amperes per unit area.

### 3. Laser and Material Parameters

Since a single photon can generate at most one electron-hole pair, long-wavelength lasers (e.g., CO and CO<sub>2</sub>) are more efficient and, therefore, narrow-gap infrared materials are of particular interest for this application. Two partial lists of CO lasing lines which would yield millimeter frequencies are given in Tables 1 and 2.

Table 1

Partial list of CO Laser Transitions with Beat Frequencies Near 240 GHz

Transition	$\lambda(\mu\text{m})$	$\nu(\text{cm}^{-1})$	Beat Frequency (GHz)	$\lambda(\text{mm})$
P(13)	5.45	1833.51		
P(14)	5.47	1829.59	237.0	1.266
P(15)	5.48	1825.61	239.7	1.252
P(16)	5.49	1821.60	241.5	1.242
P(17)	5.50	1817.56	243.0	1.235
P(18)	5.51	1813.50		

Table 2

Partial List of CO Laser Transitions with Beat Frequencies Near 95 GHz

Transitions	Beat Frequency	$\lambda(\text{mm})$	$\lambda(\mu\text{m})$
1. 11-10 P(11) and 9-8 P(24)	94.8 GHz	3.165	5.43
2. 10-9 P(23) and 9-8 P(28)	93.9 GHz	3.195	5.50
3. 9-8 P(12) and 8-7 P(19)	95.7 GHz	3.135	5.30

Equation (8) indicates that the values of absorptivity, saturation velocity and responsivity should be large for efficient current generation. A material with a large thermal conductivity would minimize the thermal problem through rapid heat conduction, which is especially important for high-power generation. In order to minimize the adverse effects of the diode capacitance and series resistance, which limit the frequency response and contribute to RF loss, the dielectric constant of the material should not be overly large but the  $N^+$ -layer doping be high. The depletion layer width which is limited because of the transit-time effect must also approximately satisfy the equation

$$W = \sqrt{\frac{2\epsilon V_b}{qN_d}} \quad (9)$$

where  $V_b$  is the bias voltage,  $N_d$  is the doping concentration of the N layer, and  $\epsilon$  is the dielectric constant. The narrow-gap mixed crystal HgCdTe appears to be a good candidate material to be used with the CO lasers operating at around 5  $\mu\text{m}$  wavelength and will be used for the configuration design. The parameter values of this material are given in Table 3.

Table 3

Parameter Values of HgCdTe at 77°K

Parameters	Values
Absorptivity ( $\alpha$ )	$\geq 10^5 \text{ m}^{-1}$
Saturation Velocity ( $V_s$ )	$4 \times 10^5 \text{ M/S}$
Dielectric Constant ( $\epsilon/\epsilon_0$ )	17
Thermal Conductivity (K)	0.2 Watt/C°/cm
Breakdown Voltage ( $V_b$ )	Greater than 2 Volt



## B. FORMULATION

A simple transmission line model may be used to understand the travelling-wave process. For the optically induced current distribution under consideration, however, waveguide configurations are more efficient for power generation because of their inherently strong source-to-field coupling characteristics. We will first develop the transmission line approach to gain some physical insights, and then develop the waveguide model.

### 1. Transmission Line Model

It is easy to show from the transmission line equations that the transverse voltage  $V$  of a transmission line driven by a travelling-wave current source with the direction of propagation along  $z$  satisfies

$$\frac{d^2 V}{dz^2} - ZYV = -ZJ'e^{-i\beta'z} \quad , \quad z_1 < z < z_2 \quad (10)$$

where  $z_1 < z < z_2$  is the source region,  $Z$  is the series impedance per unit length of the line,  $Y$  is the shunt admittance per unit length of the line,  $J'$  is the current amplitude and  $\beta'$  is the propagation constant of the current source. For convenience we have omitted the time factor  $e^{i\omega t}$  from Equation (10).

The solution of Equation (10) is given by Equation (A16) of Appendix A. The first equation of (A16) describes the voltage propagating to the left from  $z = z_1$  to the matching impedance at  $z = 0$ . Since  $\gamma$  is of the form  $\gamma = \alpha_c + i\beta$ , where  $\alpha_c$  is the loss constant and  $\beta$  is the propagation constant of the line itself, the left-going voltage is negligible when the interaction is phase-matched (i.e.,  $\beta = \beta'$ ). In contrast, the right-going voltage, as described by the third equation, is "resonantly" large for  $\beta = \beta'$ . Within the source region the voltage is described by the second equation of (A16). It has the characteristics of a growing space-transient wave, as expected, because energy is coherently added to the wave in this region.

## 2. Waveguide Model

The complex electric field  $\vec{E}$  inside a uniform metallic waveguide which is excited by a current per unit area,  $\vec{J}$ , with time variation  $e^{i\omega t}$  satisfies

$$\nabla^2 \vec{E} + k^2 \vec{E} = i\omega \mu \vec{J} \quad (11)$$

where  $\nabla$  denotes vector quantities,  $k = \omega \sqrt{\mu \epsilon}$  and  $\mu$  the permeability.  $\vec{E}$  may be expanded in terms of the waveguide eigenmodes  $\phi_{mn}$  as follows:

$$\vec{E}(x, y, z) = \sum_{m, n} A_{mn}(z) \phi_{mn}(x, y) \quad (12)$$

where  $A_{mn}(z)$  is the  $z$ -dependent "amplitude" function. Substituting Eq. (12) into Eq. (11), multiplying by  $\phi_{mn}$  and integrating over the waveguide cross section, we obtain

$$\frac{d^2 A_{mn}}{dz^2} + (k^2 - k_{mn}^2) A_{mn} = i\omega \mu \iint \vec{J} \cdot \phi_{mn} \, dx dy \quad (13)$$

$k_{mn}$  being the eigenvalue (i.e., cutoff wave number) corresponding to  $\phi_{mn}$ . For  $\vec{J} = J\hat{y}$ , (11) simplifies to:

$$\frac{d^2 A_{mn}}{dz^2} + (k^2 - k_{mn}^2) A_{mn} = i\omega \mu \iint J \phi_{mn} \, dx dy \quad (14)$$

We see that the excited mode amplitude  $A_{mn}$  is large when the overlap integral is large (i.e., strong source to field coupling). It is usually the dominant or lowest-order mode which is excited. In any case the higher-order modes have much larger loss constants and decay rapidly down the guide. We therefore assume only the dominant mode is excited and reduce Eqs. (14) and (12) to

$$\frac{d^2 A}{dz^2} + (k^2 - k_c^2) A = i\omega \mu \int_{-\frac{s}{2}}^{\frac{s}{2}} J(x) dx \quad (15)$$

$$E(x,z) = A(z) \phi(x) \quad (16)$$

where  $A(z)$  is the dominant mode amplitude,  $\phi$  is the corresponding eigenfunction and  $k_c$  is the cutoff wave number.

In deriving Eqs. (15) and (16), the following assumptions have been made:  $J$  is uniform in the transverse directions; the waveguide cross section is symmetrical about  $x = 0$  with  $J$  confined within  $-s/2 \leq x \leq s/2$ ; and the dominant mode function is  $y$ -independent. As we shall see, these assumptions are valid and appropriate for the present case.

#### C. WAVEGUIDE DESIGN AND NUMERICAL RESULTS

##### 1. Possible Configurations

Ideally, the waveguide structure coupled to the source should be wide-band, low loss, and should have a low characteristic impedance. A large bandwidth allows frequency tunability and single-mode operation, while low loss allows a longer structure to be used, which would minimize the thermal problems and thus increase power handling capability. A low impedance configuration is desirable for high-power generation since the diode is voltage limited. Here the characteristic impedance  $Z_v$  is defined as

$$Z_v = \frac{V_0^2}{2P} \quad (17)$$

where  $P$  is the average power and  $V_0$  is the maximum voltage across the guide. Additionally, the shape and dimensions of the waveguide cross section should be such to provide strong coupling between the mode fields of the waveguide and the distributed diode current source, as suggested by the overlap integral of Eq. (15). Because of the transit-time effect, however, the active HgCdTe layer thickness is necessarily limited to no more than about 2  $\mu\text{m}$ . To minimize the effect of leakage current and to simplify fabrication, the width of the strip diode is probably limited to no more than about 25  $\mu\text{m}$ . The cross sectional area



of the active layer is therefore about  $2\text{ }\mu\text{m} \times 25\text{ }\mu\text{m}$ , which is small compared to that of a standard rectangular waveguide operating in the millimeter region (i.e., 100 to 300 GHz). This suggests that a ridged rectangular guide be used, with the Schottky diode modular filling the gap above the ridge. Such a configuration would provide strong source-to-field coupling, because its dominant mode fields are known to be concentrated in the gap region. Moreover, ridge-guide structures are inherently wideband and tunable over a wide frequency range. Although these guides are more lossy than the corresponding rectangular guides, their impedances are much lower, and, therefore, they have proportionately higher output capability.

Both the single-ridge guide and the finline guide, sketched in Fig. 3, would provide strong coupling between the source and the fields, the latter corresponding to a double-ridge guide of negligible ridge thickness. For the single-ridge configuration, confinement of the millimeter energy to the gap is a key (but manageable) concern because of possible millimeter wave energy loss through the slot above the ridge. The CdTe substrate is a transparent dielectric at the  $5\text{ }\mu\text{m}$  laser wavelength, thus absorption of the laser energy, and hence carrier generation, occurs only within the HgCdTe layer. The configuration as illustrated in Fig. 4 would be a good approximation of the ideal single-ridge design, which would not be very difficult to realize. For the finline configuration the HgCdTe layer should not be doped as a conductor, so that it would behave as a dielectric and would not significantly alter the modal fields. Since the fields of these configurations are primarily concentrated in the gap region, guide walls sufficiently away from the gap may be altered for diode biasing without affecting the device performance. Various proven techniques for biasing diodes mounted in this type of structure have been reported in the literature and will not be discussed here.<sup>5</sup> Both the cutoff frequency and the characteristic impedance of these ridge guide structures are fairly well understood and can be readily calculated.<sup>6, 7</sup> Using these calculations for the ridge guide configuration neglects the guiding effects of the dielectric within the gap and thus underestimates the field-current coupling efficiency. As might be expected from the "gap" volume consideration, the single ridge guide has a lower impedance than the finline guide and, therefore, the former is superior for high power generation.

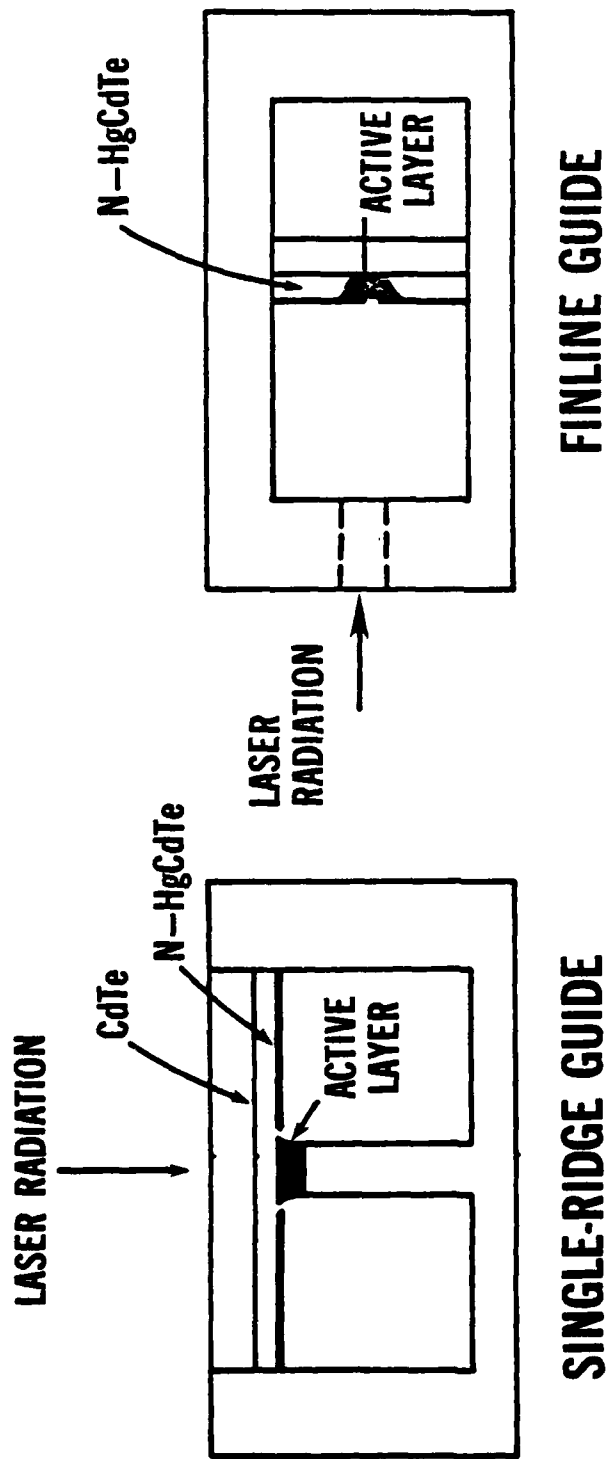


Figure 3. Cross Sectional Views of Two Low-Impedance and Wideband Waveguide Configurations (not to scale)

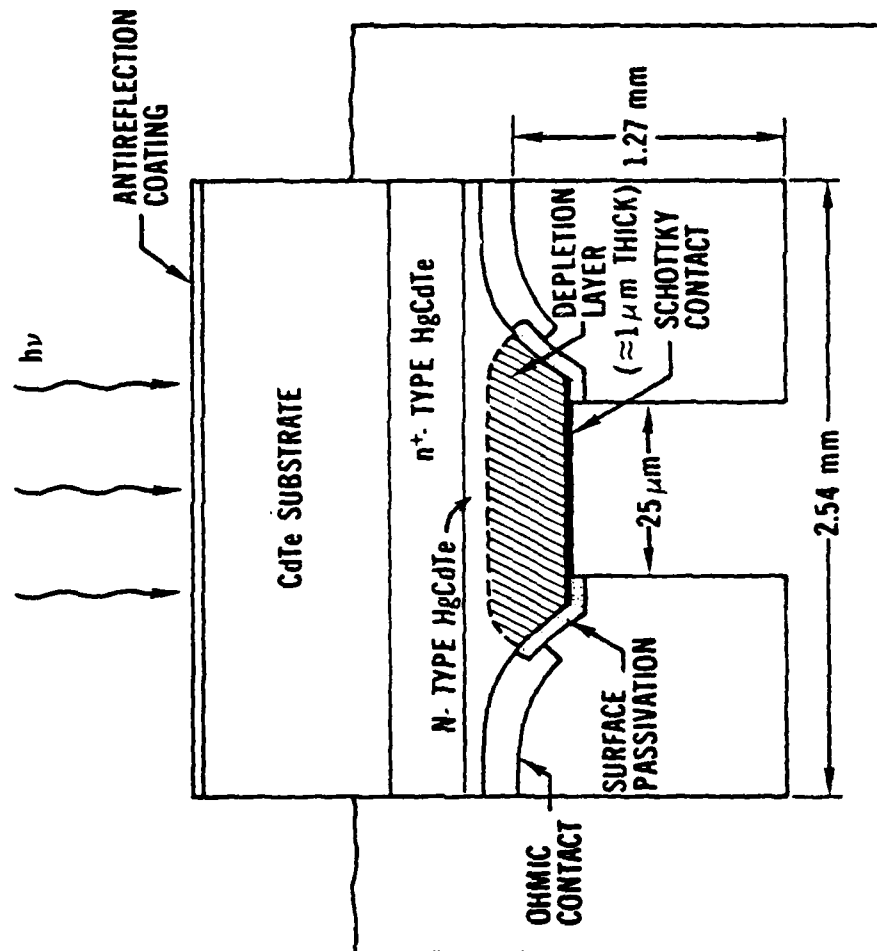


Figure 4. Single-Ridge Configuration (not to scale)

## 2. Device Performance

In this section, analysis and performance calculations are made for a single ridge configuration having a N-type HgCdTe layer as the active medium. The dominant mode eigenfunction  $\phi(x)$  is given by<sup>7</sup>

$$\phi = \begin{cases} \cos(k_c x), & -\frac{a}{2} < x < \frac{a}{2} \text{ and } -d < y < 0 \\ 0, & \text{elsewhere} \end{cases} \quad (18)$$

Substituting Eq. (18) and the expression for the travelling-wave current into Eq. (15), we have:

$$\frac{d^2 V_0}{dz^2} - \gamma^2 V_0 = i\omega\mu \frac{I_0 e^{-i\beta'z}}{lS} d \frac{2\text{sinc}(k_c S/2)}{1 + \text{sinc}(k_c S)} \quad (19)$$

where  $V_0 = Ad$ , the maximum voltage across the guide,  $I_0$  is the laser-induced millimeter current amplitude in the strip diode,  $\text{sinc} x = \sin x/x$ ,  $-\gamma^2 = k^2 - k_c^2 = (\alpha_c + i\beta)^2$ , and  $l$  is the active layer length extending from  $z = 0$  to  $z = l$  along the guide axis. The output power of the device,  $P$ , is

$$P = \frac{V_0^2(z=l)}{2Z_v} \quad (20)$$

$V_0$  as a function of  $z$  in the active region  $0 \leq z \leq l$  is found from the Green's function technique of Appendix B to be

$$V_0 = \frac{Z_0 d I_0}{lS} \left[ \frac{\text{sinc}(k_c S/2)}{1 + \text{sinc}(k_c S)} \right] \left[ \frac{e^{-i\beta z}}{i\delta\beta - \alpha_c} (e^{-i\delta\beta z} - e^{-\alpha_c z}) \right. \\ \left. + \frac{e^{i\beta z}}{i2\beta} (e^{-i2\beta l} - i\delta\beta l - \alpha_c(l-z)) e^{-i2\beta z - i\delta\beta z} \right] \quad (21)$$

where we have substituted  $\beta + \delta\beta$  for  $\beta'$  and  $z_1 = 0$  and  $z_2 = l$ . For the ideal phase-matched case, where the current source and the mode fields are in perfect synchronism,  $\delta\beta = 0$ . We have also made the usual assumption that  $\alpha_c, \delta\beta \ll \beta$

which is valid for most cases of practical interest. Wavevector mismatching,  $\delta\beta$ , may result from misalignment between the lasers or with respect to the waveguide axis. The effect of misalignment on the wavevector is quantitatively studied in Appendix C.

The millimeter power at points along the active region for frequencies 100, 150 and 200 GHz is shown in Figures 5 and 6. The active length, height and width of the strip diode used in the calculation are, respective,  $l = 5 \text{ } \mu\text{m}$ ,  $S = 25 \text{ } \mu\text{m}$  and  $d = 1 \text{ } \mu\text{m}$ . These values were chosen from a tradeoff study, taking into account the effect of both transit-time and heat generation, as well as the state-of-the-art HgCdTe technology. The induced millimeter current amplitude  $I_0$  in the active region is 2 amp, which corresponds to about 1 watt of optical power from each of the two CO lasers. For each frequency the values of  $\lambda_c$ ,  $\beta$ ,  $k_c$ ,  $\alpha_c$  and  $Z_v$  corresponding to the waveguide a and b dimensions were calculated from references.<sup>6, 7, 8</sup> These and other parameter values are given in Table 4.

Table 4

Partial List of Parameter Values used in the Calculations

f(GHz)	$\lambda_c(\text{M})$	$\beta(\text{M}^{-1})$	$k_c(\text{M}^{-1})$	$\alpha_c(\text{M}^{-1})$	$Z_v(\text{OHMS})$	axb(mm x mm)	Standard Waveguide Designation
200	0.016	$1.7 \times 10^4$	383	39	2.72	1.295 x 0.6475	WR5
150	0.021	$1.3 \times 10^4$	298	27	2.69	1.650 x 0.8255	WR6
100	0.033	$8.6 \times 10^3$	192	14	2.65	2.540 x 1.2700	WR10

In order for the device to have gain, the applied DC voltage must exceed the AC voltage generated by the propagating millimeter wave. DC voltages for three selected power levels are also shown in Figures 5 and 6. For example, if 2 watts of output power is required, the diodes must be reverse biased to at least 4 volts.

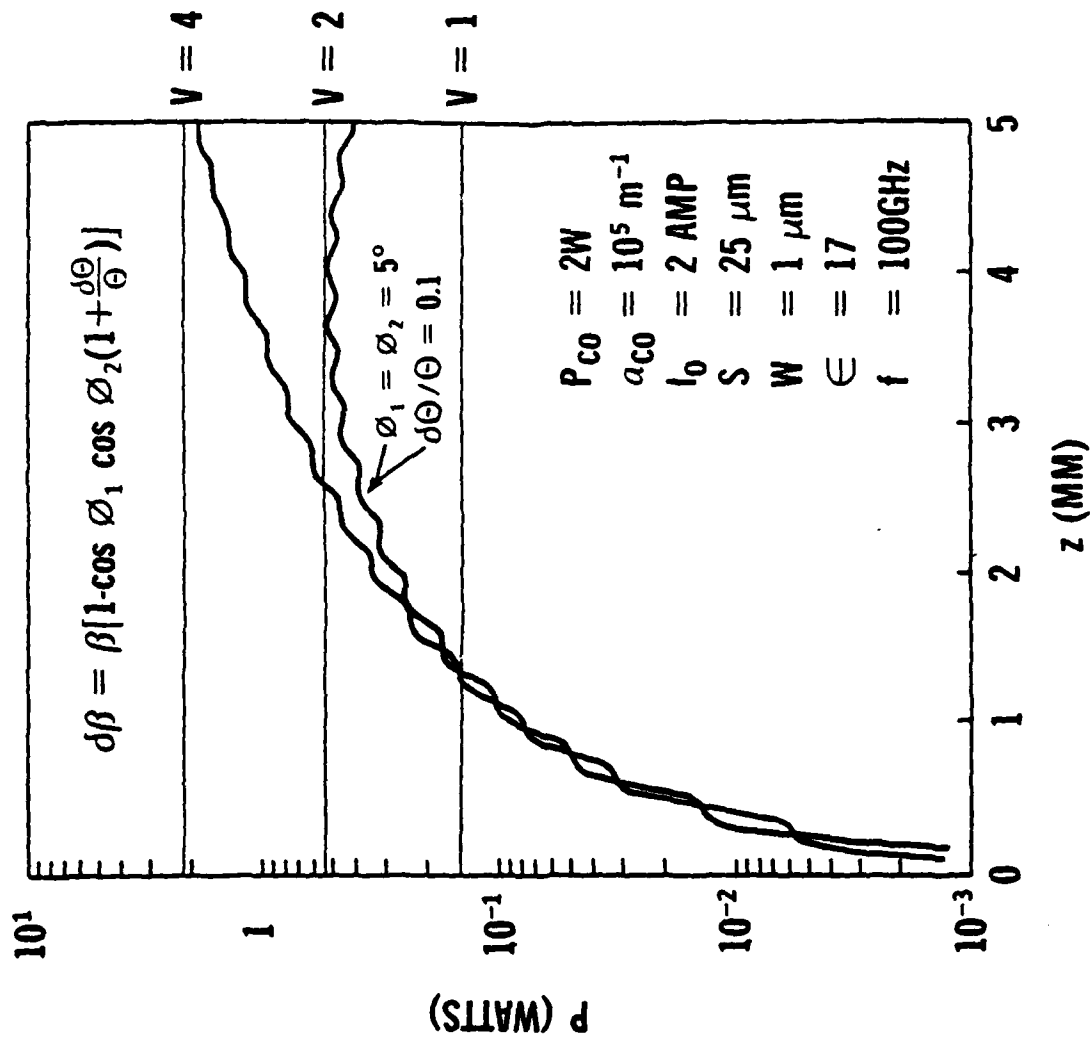


Figure 5. Millimeter Power Along the 5 mm Long HgCdTe Layer in Gap of Single-Ridge Guide at  $77^\circ$  with Impedance Matched: Upper Curve is for the Phase-Match Case, While Lower Curve Shows Effect of Phase Mismatch Due to Laser Misalignment

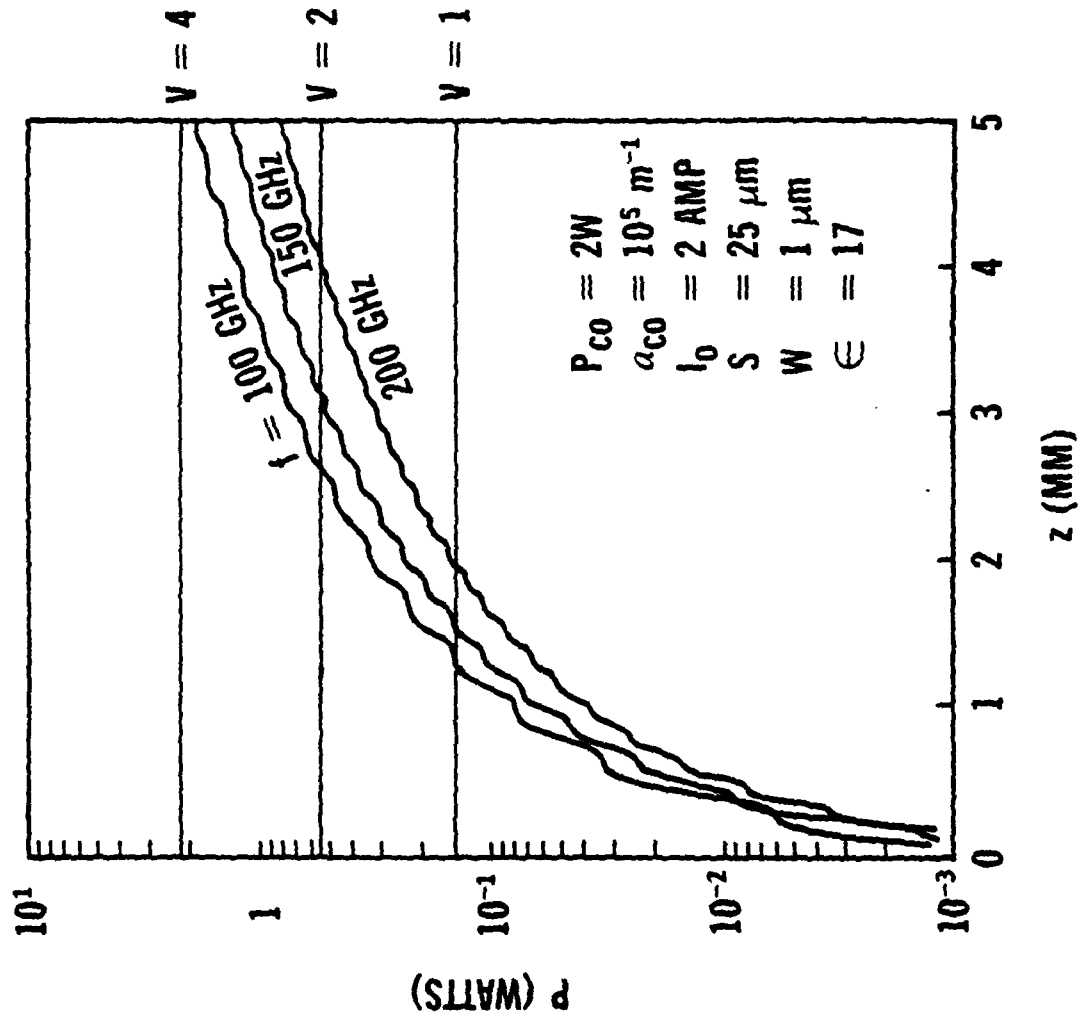


Figure 6. Millimeter Power P Along the 5 mm HgCdTe Active Region in Gap of Single-Ridge Guide at 77° K with Impedance and Phase Matched (see Table 4 for the Other Parameter Values)



Figure 5 shows the effect of the phase-mismatch error due to laser misalignment as discussed in Appendix C. The output power of the device, which is the value of  $P$  at  $z = \lambda$ , is relatively insensitive to the orientation angles  $\phi_1$  and  $\phi_2$  for angle values smaller than about  $10^\circ$ . However, the output power is sensitive to the error in  $\theta$ , especially at higher frequencies. The 10% error in  $\theta$  used in the calculation is probably large, for the nominal values of  $\theta$  are on the order of milliradians and therefore much smaller error should be achievable experimentally. Figure 6 shows that the output power is relatively insensitive to frequency, implying that the device has frequency-tunable characteristics. Since it is proportional to the square of the total current, the output power would increase rapidly with increasing current or with laser power.



### 3.0 EXPERIMENTS OF THE LASER-INDUCED CONCEPTS

Two experiments were conducted to verify the laser-induced concept of millimeter wave generation by laser intensity modulation in diode/waveguide structures.

In the first experiment, we successfully verified the modulation concept using a point-like diode structure.<sup>10</sup> In the second experiment, an unsuccessful attempt was made to verify the traveling-wave concept using a layered diode of 5-mm in length. Both experiments are described in this chapter.

#### A. POINT-DIODE EXPERIMENT

This section describes the experiment which was conducted to verify the concept of millimeter wave generation by laser intensity modulation in a point diode structure. A point-source  $\text{Hg}_{1-x}\text{Cd}_x\text{Te}$  diode operating at 77°K was used in the experiment. This diode was fabricated on a 10- $\mu\text{m}$ -thick epitaxial  $\text{HgCdTe}$  layer grown on a transparent  $\text{CdTe}$  substrate.<sup>11</sup> Optical intensity modulation at the millimeter frequency was provided by the interference of two overlapping CO lasers oscillating at 5.467  $\mu\text{m}$  and 5.478  $\mu\text{m}$  wavelengths. Figure 7 is a photograph of the two CO lasers constructed for this experiment. As expected, the output millimeter frequency was equal to the laser beat of 110 GHz.

The  $\text{Hg}_{1-x}\text{Cd}_x\text{Te}$  diode structure is depicted in Figure 8. The  $x$  value was chosen to be 0.26. For this  $x$  value the absorption edge of the interband transition is 6.5  $\mu\text{m}$  at 77°K, implying that the layer is highly absorptive to the CO laser radiation.<sup>12</sup> The substrate was first lapped to a thickness of 125  $\mu\text{m}$  and an  $n^+$  region was implanted on the epilayer surface using boron atoms at 100 keV.<sup>13</sup> The implantation caused a damaged  $n^+/p$  junction of 3 to 5  $\mu\text{m}$  in thickness below the  $n^+$  surface. After an indium-metallization of the  $n^+$  surface, the implanted layer was then mesa-etched to define the diode, as shown in Figure 8. In order to reduce the surface leakage current and series resistance, photolithographic techniques were also employed to passivate the junction edge with  $\text{ZnS}$ , and to make an  $\text{Au/Sn}$  ohmic contact to the p-layer close to the active chips, each containing a ring-shape diode, for mounting in the mm-wave waveguide.



Figure 7. Photograph of the Waveguide CO Lasers

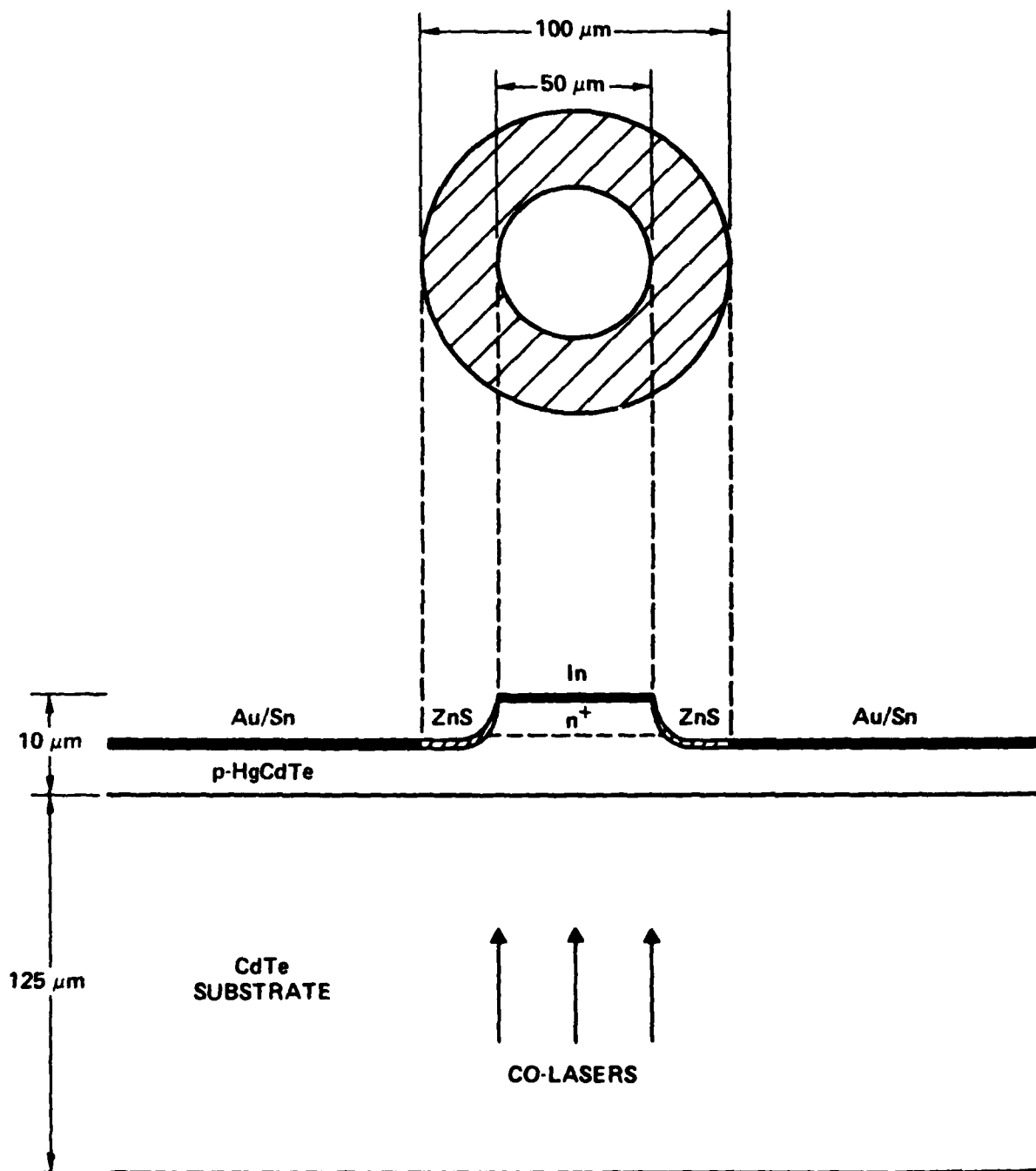


Figure 8. Top and Cross Sectional View of the Heterostructure  $n^+/p$  HgCdTe Photodiode (The thickness of the epitaxial layer is not drawn to scale.)

The diode has a reverse leakage current on the order of nanoamperes and a breakdown voltage of 2 to 3 volts at 77°K. Its infrared spectral response shows a cutoff wavelength between 6.0 and 6.5  $\mu\text{m}$ . The junction capacitance measured at a reverse bias of 0.5 volt is 0.15 pF, implying that the depletion region is 2  $\mu\text{m}$  wide. In the absence of laser radiation, the series resistance of the diode is 200 ohms, measured under forward-biased conditions. However, it reduces to less than 10 ohms when the laser is applied, apparently due to excited carriers between the diode and the ohmic contact. Therefore, the RC cutoff frequency is enhanced by laser illumination to beyond 100 GHz. This suggests that the effective conductivity of the undepleted portion of the HgCdTe layer in a distributed configuration would also increase significantly under laser illumination, thus minimizing the loss of millimeter energy.

The modulator/waveguide structure is depicted in Figure 9. The diode chip is mounted on a Be-Cu post inserted in the reduced-height mm-waveguide of dimensions 0.3 mm  $\times$  2.5 mm. The lasers are incident from the backside of the diode via a small cone machined in the sidewall of the waveguide. The diode is connected by a gold wire bonded on the  $n^+$  surface to a thin-film choke for dc bias and monitor. Efficient coupling between the diode and the waveguide fundamental mode is accomplished by the choke, a mechanically tunable backshort and a four-step impedance transformer leading to a conventional WR-10 waveguide.<sup>14</sup> The generated mm-wave then propagates in a stainless steel waveguide to a room-temperature crystal rectifier (sensitivity 500 V/W) for detection. Vacuum seal is made using a  $\text{CaF}_2$  laser window and a 0.001-inch-thick Mylar window in the waveguide flange. The response of the HgCdTe diode to a weak broadband infrared signal is shown in Figure 10(a). In order to test the coupling between the diode and the mm-waveguide, a 95-GHz signal from an IMPATT oscillator is injected into the Dewar via the stainless steel waveguide. The diode dc response to such an mm signal is shown in Figure 10(b) where the I-V curves are taken with increasing RF power, suggesting that this device may be useful also as a sensitive detector for millimeter radiation. The observed video detection is due to rectification expected from the nonlinear exponential characteristics of the forward-biased HgCdTe diode.

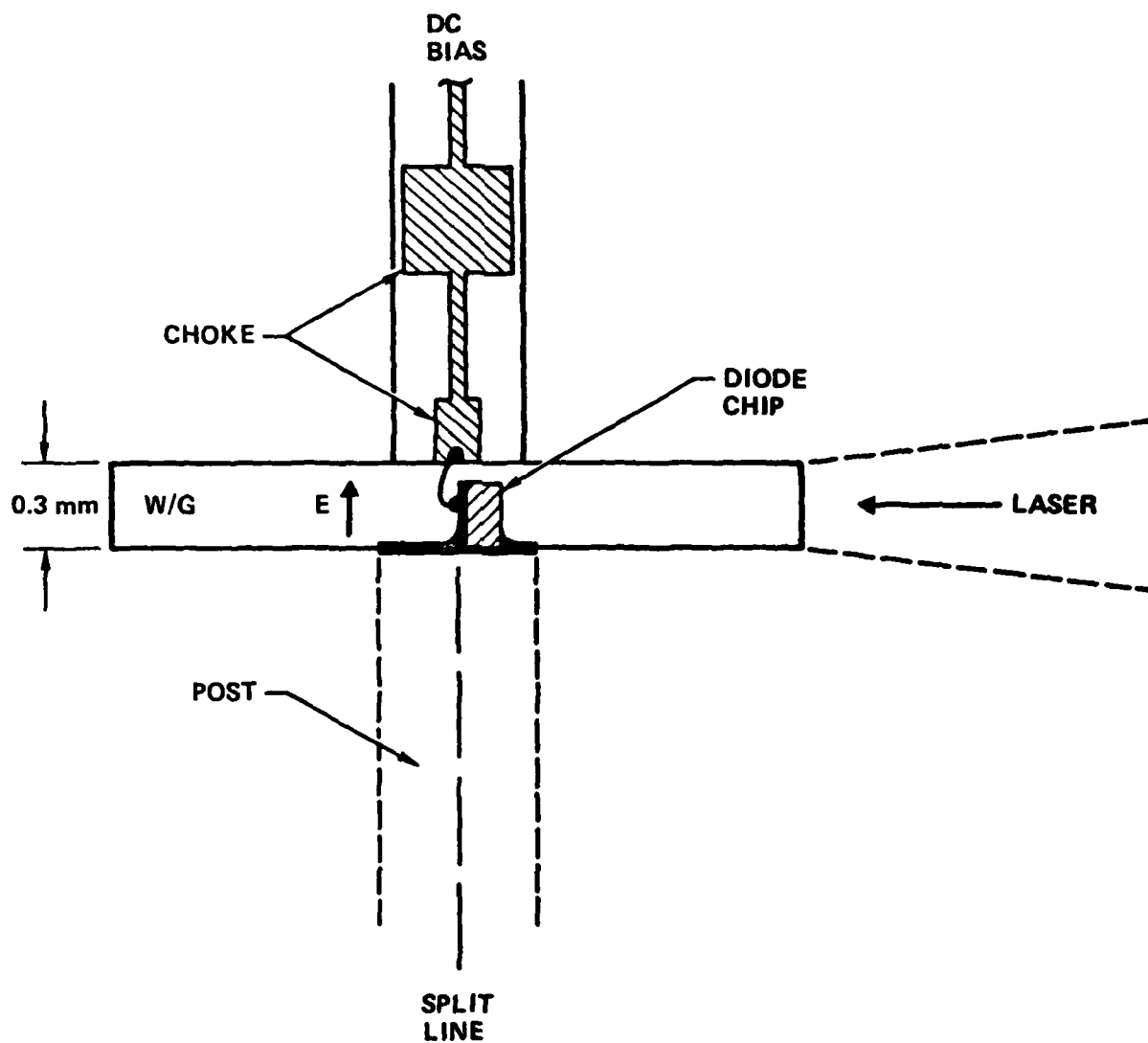
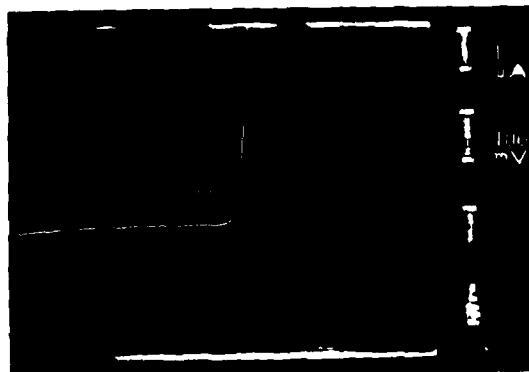
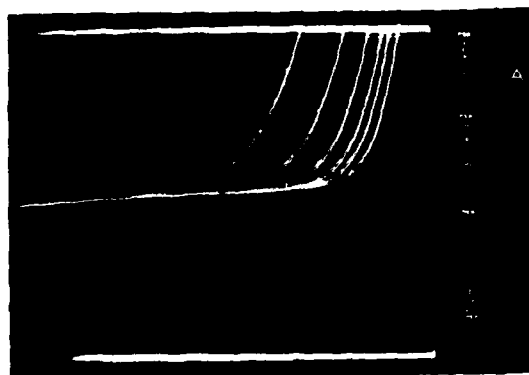


Figure 9. Diode Chip Mounted in a Reduced-Height mm-Wave Waveguide  
(The longer dimension of the waveguide is 2.54 mm.)



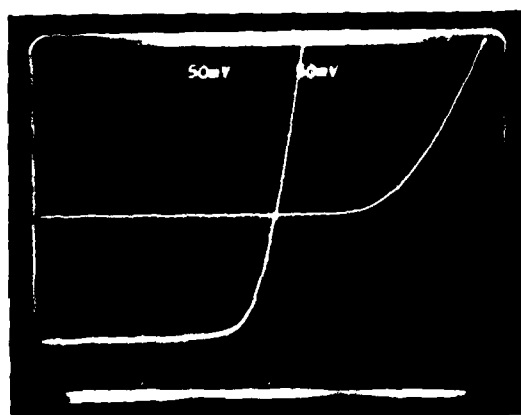
(a)

Diode I-V curves without (top) and with (bottom) a weak infrared input.



(b)

Diode I-V curves in the presence of a 95 GHz input signal. The rf power is zero for the curve on the right, and is 0.1, 0.2, 0.4, 0.8, and 1.6  $\mu\text{W}$ , respectively, for subsequent curves to the left.



(c)

Diode characteristics when the laser radiation is applied. The vertical scale should be 0.5 mA/div., since the current is measured by a 100-ohm resistor in series with the junction.

Figure 10. Diode I-V Curves and Characteristics

The experimental setup for millimeter wave generation is as depicted in Figure 2, a photograph of which is given in Figure 11. Two waveguide CO lasers oscillating at 5.467  $\mu\text{m}$  and 5.478  $\mu\text{m}$  wavelengths were combined to produce a beat of 110 GHz. For each of the lasers, single-line operation and line control were accomplished with an intracavity grating, with laser output power of about 100 mW. The beams were combined with a 50-percent beamsplitter and focused in the liquid nitrogen Dewar housing the diode/modulator structure. When the modulator was illuminated by the laser, a relatively large dc photocurrent and a significant reduction in the forward resistance were observed [see Figure 10(c)]. When the absorbed laser power was sufficiently large to produce a dc photocurrent of about 10 mA, an mm-wave signal was detected at the output of the crystal rectifier. The maximum mm-wave output was 0.75  $\mu\text{W}$ , observed when the HgCdTe diode was reverse-biased at 0.5 volt in the flat region of the I-V curve before breakdown. The frequency of the generated mm-wave was verified from the backshort tuning to be consistent with the laser line separation (110 GHz). Although the laser-induced dc photocurrent was about 10 mA, the millimeter current was only about 100  $\mu\text{A}$ . For this millimeter current value, the observed output power of about 1  $\mu\text{W}$  is approximately in agreement with calculations. Several factors limited the millimeter current amplitude, including laser misalignment (cross polarization), photo absorption outside the depletion layer, carrier velocity saturation, and the decrease of quantum efficiency with increasing frequency. However, these adverse effects would be minimized with a distributed configuration and therefore higher device efficiency and output power would result.

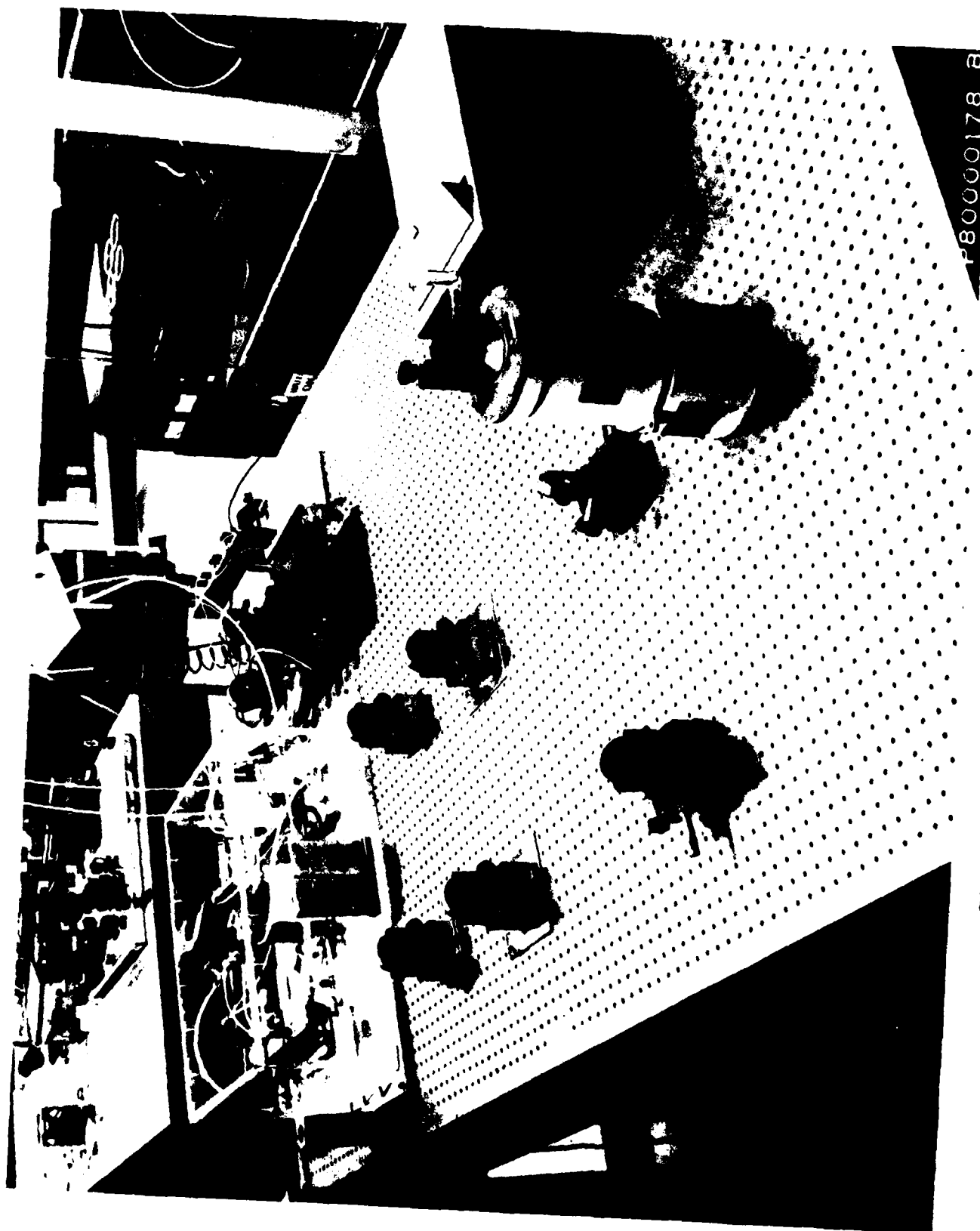


Figure 11. Photograph of Millimeter Experimental Setup



## B. DISTRIBUTED-DIODE EXPERIMENT

This section summarizes the effort on the distributed diode experiment. As previously mentioned, the purpose of this experiment was to demonstrate the traveling-wave concept. However, we were unsuccessful in fabricating a strip diode after several attempts, and therefore the concept demonstration could not be made.

Even though we were unable to demonstrate the merit of the traveling-wave concept, we have learned a great deal from our developmental effort, particularly in diode design and fabrication techniques. In what follows we will summarize the results.

The distributed diode/waveguide configuration which we have attempted is sketched in Figure 12. It is basically a finline structure housed in a rectangular waveguide, with the diode in the finline slot. The configuration is designed for operation at 100 GHz, and its dimensions are based upon the analysis and tradeoff results obtained in Chapter II. A photograph of the configuration components is given in Figure 13.

The active finline structure and its supporting quartz substrate are sketched in Figure 14. The active region has a  $1\mu$  gap and a 5-mm length. Impedance matching is provided by the metallic exponential tapers. These tapers are about 4 guide wavelengths long and should provide extremely good matching, as suggested by the calculations shown in Figure 15.

The metallic tapers on the quartz substrate as well as the active finline structure were fabricated via photolithograph. Partly due to the poor quality HgCdTe diode materials which were available to us and partly due to our limited experience working with the materials, we were not successful in fabricating a strip diode. A photograph of a typical fineline/diode "fabricated" is shown in Figure 16. Figures 17 and 18 are photographs of a typical HgCdTe sample.

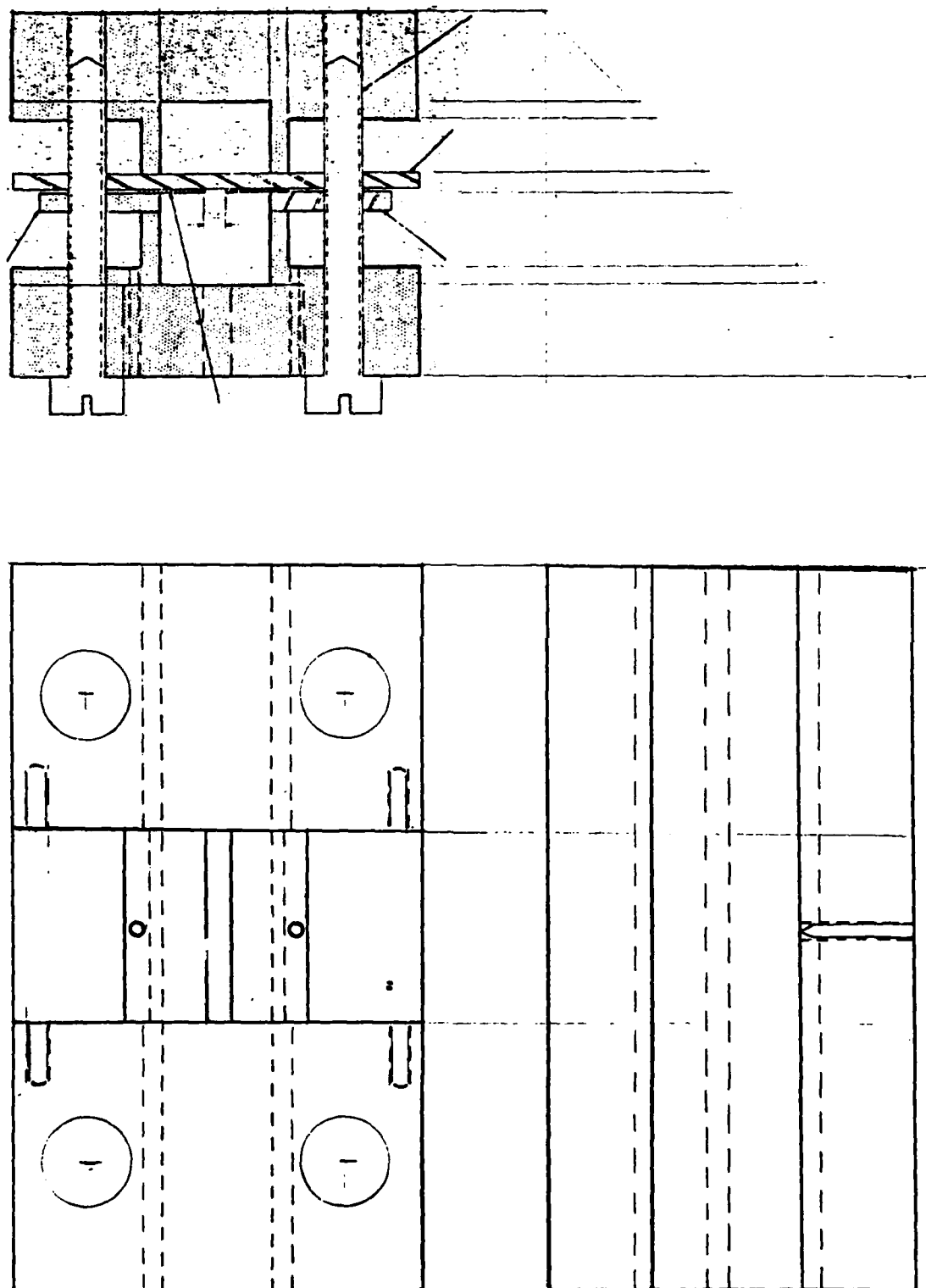


Figure 12. Finline Guide Drawing (not to scale)

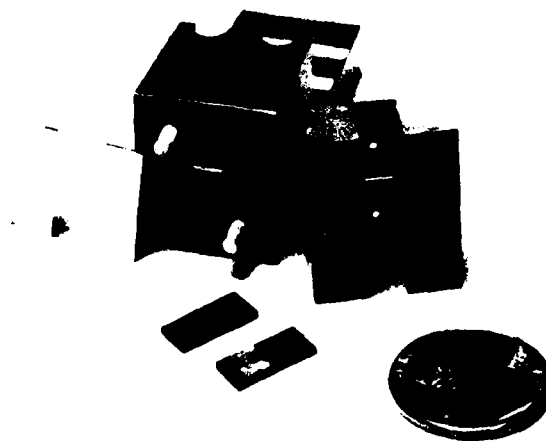


Figure 13. Photograph of Distributed Diode/Waveguide Configuration  
(This design is for operation at 100 GHz.)

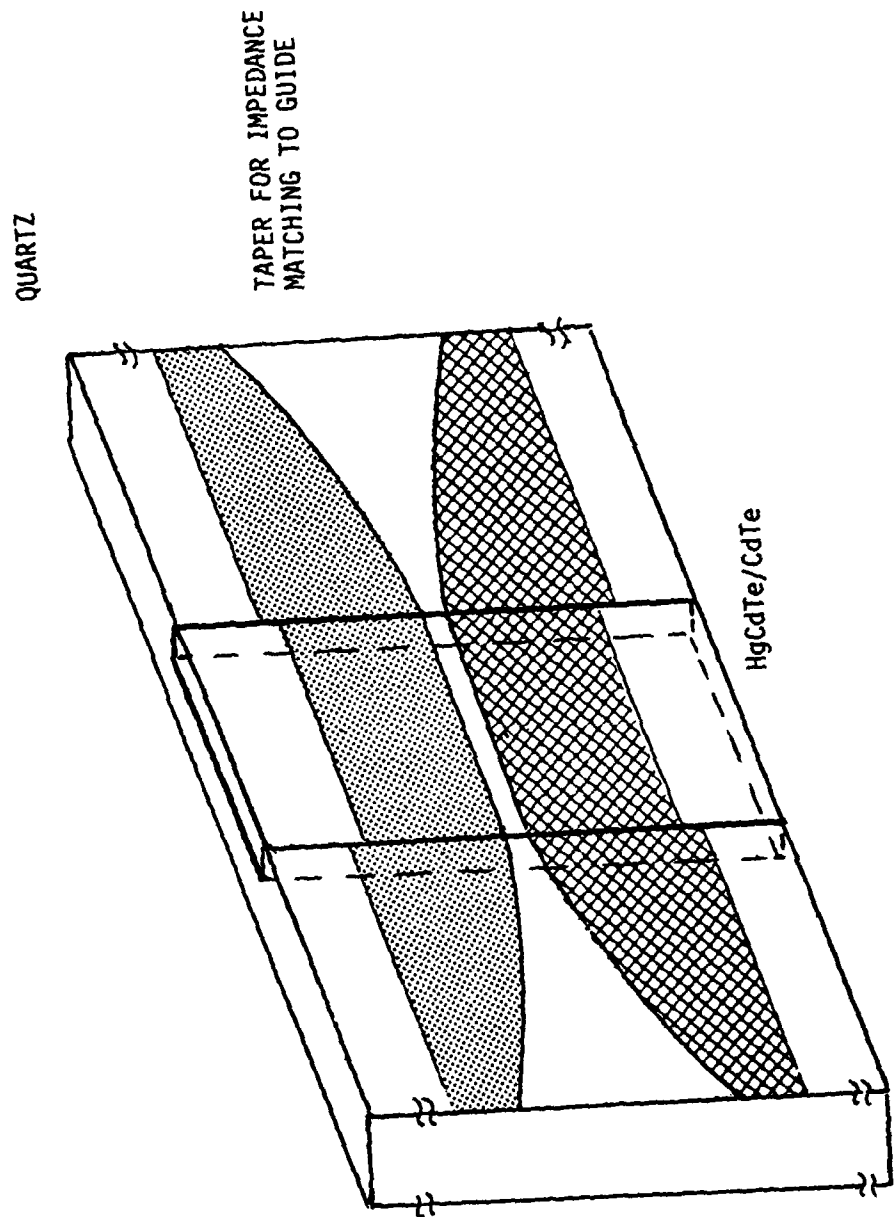


Figure 14. Quartz ( $\text{SiO}_2$ ) Holder and HgCdTe/CdTe Strip Diode

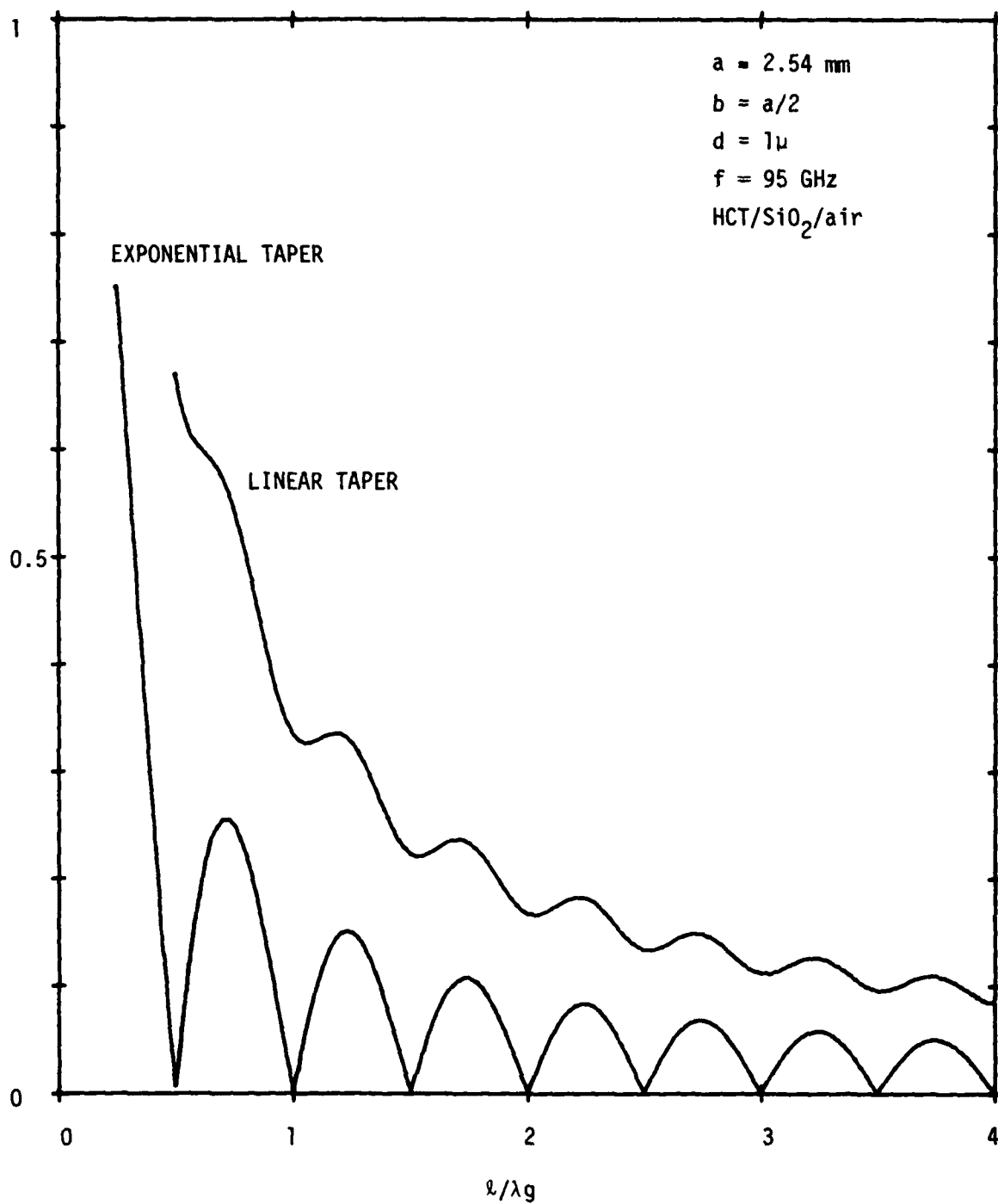
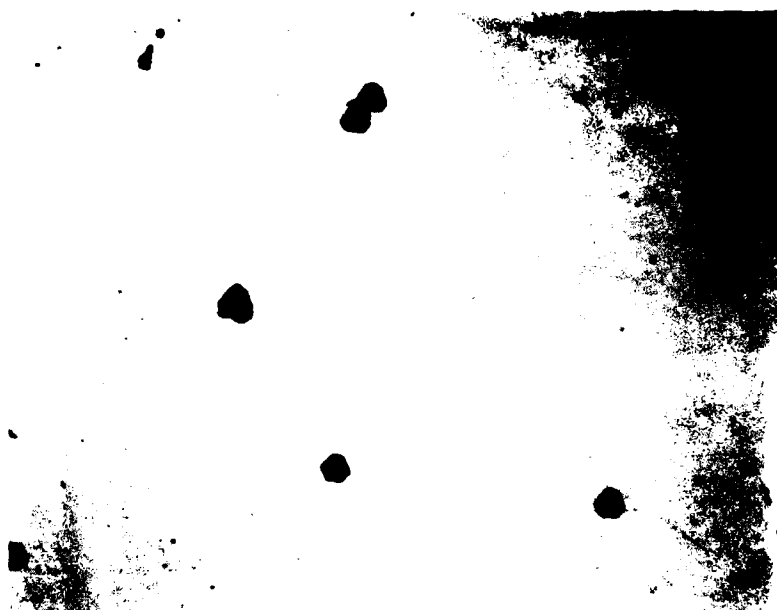


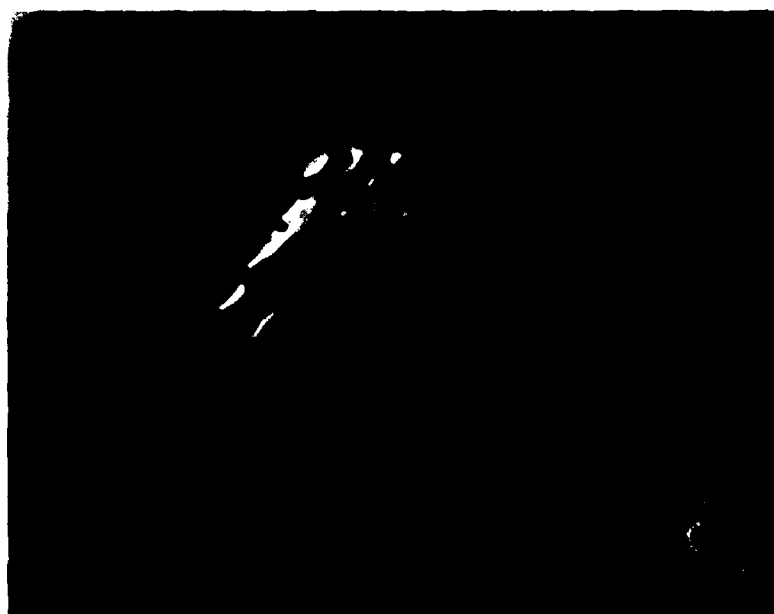
Figure 15. Amplitude Reflection Coefficient ( $r$ ) Vs. Normalized Taper Length ( $l/\lambda_g$ ) (Finline)



Figure 16. Photograph of a Broken Diode/Finline Structure



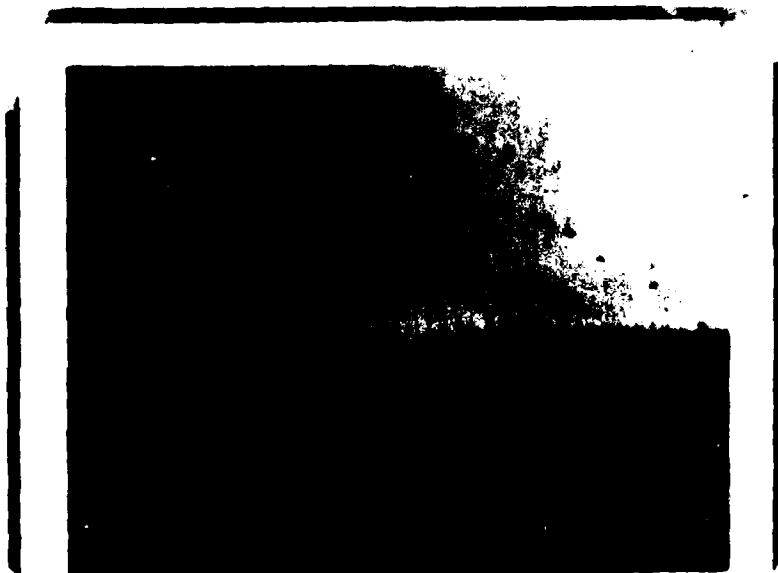
↓  
—  
— 100μ  
↑



—  
↑  
  
100μ  
  
↓  
—

Figure 17. Photographs of Typical HgCdTe Sample Surface  
(see reference scale)

EDGE VIEW



↓  
—  
10μ  
—  
↑

TOP VIEW



↑  
—  
100μ  
—  
↓

Figure 18. Photographs of Typical HgCdTe Sample





#### 4.0 TRAVELLING-WAVE IMPATT MODE IN A RIDGEGUIDE CONFIGURATION

In this chapter the preliminary analytical results we have obtained for a distributed IMPATT diode/waveguide structure are presented. The structure consists of an elongated, layered, Read-type diode in the gap of a ridge guide, very similar to the single-ridge configuration of Figure 4. The layered diode is sandwiched between and metallurgically bonded to the guide ceiling and ridge. This particular configuration is chosen mainly because of its inherently strong current-to-field coupling characteristics. As in point-like IMPATT diodes, the source current is a consequence of the avalanche effect when the diode is reverse bias at saturation. In this efficient-coupling configuration, however, the field-current interaction induces a growing travelling wave which extracts energy from the DC bias.

Although several workers have studied the distributed IMPATT mechanism in a parallel-plate configuration, no such study has been made for a ridgewaveguide configuration. Medford and Bowers actually constructed a parallel-plate configuration and observed travelling-wave behavior.<sup>15</sup> However, the observed RF gain

was very small, probably due to the inherently weak current to field coupling in a parallel-plate structure. Using the transmission line approach, Davydova, et. al. subsequently analyzed the parallel-plate configuration and found qualitative agreement with the findings of Medford and Bowers.<sup>16</sup> Robson and Hambleton also analyzed the parallel-plate configuration using the equivalent negative conductivity approach.<sup>17</sup> More recently, Franz and Beyer presented a detailed analysis of the parallel plate configuration, by considering the interaction of the avalanche carriers with the field in the active region.<sup>9</sup> As previously mentioned, the present work is on the IMPATT gain and travelling-wave behavior in a ridge-guide configuration.

As originally suggested by Read, the diode under operating condition may be considered as consisting of two adjacent layered regions: a negligibly thin layer where avalanche carriers are generated and a region where these carriers drift at their saturation velocity. In a  $P^+NN^+$  Read diode, for

example, the avalanche region is located just inside the N region next to the  $P^+N$  junction, while the drift region is the rest of the depleted N layer. The total current in the drift region of such a  $P^+NN^+$  structure is primarily the electron current, or the majority current, because the holes generated are quickly swept into the  $P^+$  region. For a  $N^+PP^+$  diode, on the other hand, hole current predominates in the drift region.

Following Read's approach and considering an elongated  $P^+NN^+$  structure, we may write the Read equation for the current density  $J_T$  in the avalanche layer as follows:<sup>18</sup>

$$\frac{\tau_1}{2} \frac{dJ_T}{dt} = J_T \left[ \int_0^y a dy - 1 \right] + J_S \quad (22)$$

where  $\tau_1$  is the transit time across the avalanche region of thickness  $y_1$ ,  $a$  is the ionization constant, and  $J_S$  is the saturation current density.

Solving Equation (22) and the appropriate Maxwell's equations for an active ridgeguide configuration, we found from our preliminary formulation and small-signal analysis that the mode amplitude of the excited travelling wave,  $A$ , satisfies the equation:

$$\frac{d^2 A}{dz^2} - \left[ -\beta^2 + a_c^2 - g' + i(2\beta a_c - g'') \right] A = 0 \quad (23)$$

where  $\beta$  and  $a_c$  are, respectively, the propagation constant and the loss constant of the unperturbed mode,  $g'$  and  $g''$  are

$$g' = \frac{2(M+1)}{\tau_1} \mu \frac{J_c}{E_c} \frac{\sin \omega \tau}{\omega \tau} \cos \omega \tau / 2 \quad (24)$$

$$g'' = \frac{2(M+1)}{\tau_1} \mu \frac{J_c}{E_c} \frac{\sin^2 \omega \tau / 2}{\omega \tau / 2}$$

In Equation (24),  $J_c$  is the DC current density,  $E_c$  is the critical DC field,  $\tau_1$  is the transit time across the drift region,  $\omega$  is the millimeter frequency,  $\mu$  is the permeability,  $M$  is the ionization index ( $\sim 6$ ) as defined by Read.<sup>18</sup>

From Equations (23) and (24) the gain constant of the travelling wave,  $G_a$ , is approximately given by

$$G_a = a_c - g'' / 2\beta M^{-1} \quad (25)$$

To estimate the magnitude of the gain constant, we consider a Si diode in the single-ridge configuration designed for 100 Hz operation. The Si parameter values are (MKS units)  $\epsilon = 11.8$ ,  $E_c = 3 \times 10^7$ ,  $J_c = 10^8$ ,  $V_s = 10^5$  and  $W = 1.5 \times 10^{-6}$ . The calculated waveguide parameter values are  $\beta = 7.16 \times 10^3$ ,  $\alpha_c = 11.66$ ,  $Z = 3.18$ ,  $\tau = 1.5 \times 10^{-11}$  and  $\tau_1 = 5 \times 10^{-13}$ . For these values the gain constant is calculated to be about 15 db per millimeter. The estimated gain constant for GaAs is about the same. Other materials, such as Ge, GaP etc., are also being considered for possible use.

To summarize, our preliminary results indicate that the ridgeguide traveling-wave IMPATT is by far much more efficient than the parallel-plate configuration previously studied.

## 5.0 CONCLUSIONS

### A. LASER-INDUCED DISTRIBUTED CONFIGURATION

As a solid-state millimeter source, the laser-induced distributed-source configuration is attractive for at least three reasons. It has high device efficiency, it has high output-power characteristics, and it is potentially compact and lightweight. There are two factors contributing to high device efficiency. First, in the configuration examined

the laser-induced current which synchronously excites the structure to generate millimeter waves is directly proportional to the laser modulation. With the interference technique, it is theoretically possible to convert 50 percent of the total laser power into the modulation. Second, the current-to-field coupling is inherently strong in the ridge guide structure, because the Schottky-diode modulator, where the millimeter current is induced, occupies the gap region in which the mode fields are concentrated. Perhaps as significant, the calculation indicates that a dielectric-loaded ridge waveguide should provide excellent coupling to other solid-state oscillators. As for the high-power output, analysis and tradeoff study indicate that CW output in the multiwatt range should be realizable providing cooling of the diode material is adequate. Thus far we have only investigated the diode material HgCdTe in some detail. Other materials (for example, InSbAs) may possibly provide better device performance.

### B. RIDGEGUIDE DISTRIBUTED IMPATT CONFIGURATION

Our preliminary analysis and calculation indicate that the ridgeguide distributed IMPATT configuration is potentially a very high-gain and efficient millimeter source. It is by far superior to the parallel-plate IMPATT configuration analyzed by Franz and Beyer.<sup>9</sup> This is not unexpected because the current-to-field coupling is much stronger in the ridgeguide structure. As compared to the laser-induced distributed configuration, the ridgeguide distributed IMPATT is much easier to implement and incorporate in a system. This is so because its operation requires only a DC battery (i.e., similar to point-like IMPATT operation) and avoids the usual alignment and stability problems associated with optical excitation.

# APPENDIX A. TRANSMISSION LINE MODEL

From Eq. (10) the transverse voltage  $V$  satisfies

$$\frac{d^2 V}{dz^2} - ZYV = -ZJ' e^{-i\beta' z}, \quad z_1 < z < z_2 \quad (A1)$$

We will solve Eq. (A1) using the Green's function technique by first finding the voltage response  $G(z, z')$  to a point current source at  $z'$  on an arbitrarily terminated line. Referring to Fig. A1,  $G(z, z')$  satisfies

$$\frac{d^2 G}{dz^2} - ZYG = -Z\delta(z - z') \quad (A2)$$

where the delta function  $\delta(z - z')$  denotes the unit point current source at  $z = z'$ . In the figure,  $Z_0$  is the characteristic impedance of the line;  $Z_1$  and  $Z_2$  are the terminating impedances at  $z = 0$  and  $z = l$ , respectively;  $V_i$  and  $I_i$ ,  $i = 1$  or  $2$ , are the voltages and currents. The voltage  $V$  due to the travelling current is

$$V(z) = \int_0^l G(z, z') J' e^{-i\beta' z'} dz' \quad (A3)$$

For notation convenience we define

$$G(z, z') = \begin{cases} V_1(z, z') & \text{for } 0 < z < z' \\ V_2(z, z') & \text{for } z' < z < l \end{cases}$$

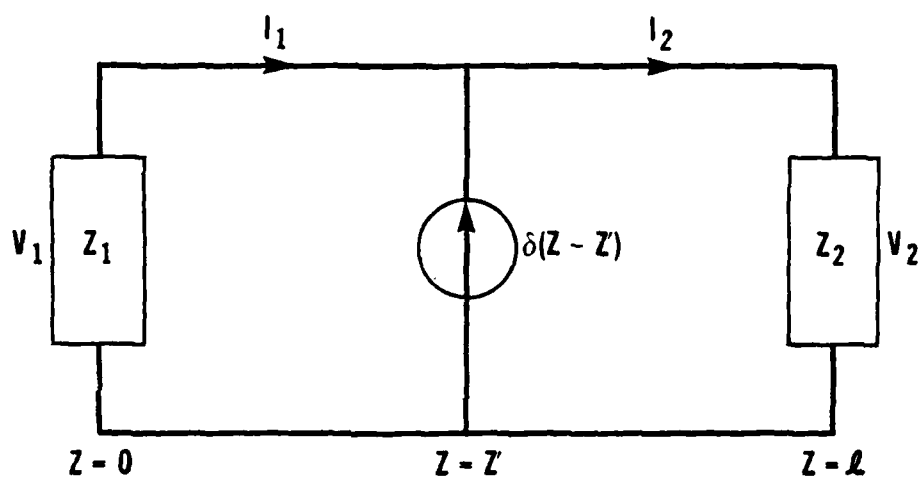


Figure A-1. Diagram of an Arbitrarily Terminated Transmission Line

The solution of Eq. (A2) for  $0 < z < z'$  is simply

$$V_1 = V_{11} e^{\gamma z} + V_{12} e^{-\gamma z} \quad (A4)$$

where  $\gamma = \sqrt{ZY}$ . Physically,  $V_{11} e^{\gamma z}$  is the left-going voltage wave while  $V_{12} e^{-\gamma z}$  is the right-going voltage wave in the region  $0 < z < z'$ . The corresponding current  $I_1$  is

$$I_1 = -\frac{V_{11}\gamma}{Z} e^{\gamma z} + \frac{V_{12}\gamma}{Z} e^{-\gamma z} \quad (A5)$$

The voltage reflection coefficient,  $\rho_1$ , at  $z = 0$  is

$$\rho_1 = \frac{Z_1 - Z_0}{Z_1 + Z_0} \quad (A6)$$

Eqs. (A4) and (A5) now simplify to

$$\begin{aligned} V_1 &= V_{11} e^{\gamma z} (1 + \rho_1 e^{-2\gamma z}) \\ I_1 &= \frac{V_{11}}{Z_0} e^{\gamma z} (\rho_1 e^{-2\gamma z} - 1) \end{aligned} \quad 0 < z < z' \quad (A7)$$

where  $V_{11}$  will be determined from the source conditions at  $z = z'$ . In a similar fashion the voltage  $V_2$  for  $z' < z < l$  is

$$V_2 = V_{21} e^{\gamma z} + V_{22} e^{-\gamma z} \quad (A8)$$

and the current  $I_2$  is

$$I_2 = -\frac{V_{21}\gamma}{Z} e^{\gamma z} + \frac{V_{22}\gamma}{Z} e^{-\gamma z} \quad (A9)$$

where  $V_{21} e^{\gamma z}$  and  $V_{22} e^{-\gamma z}$  are the left-going and right-going voltage waves, respectively. Since the voltage reflection coefficient  $\rho_2$  at  $z = l$  is

$$\rho_2 = \frac{V_{21}}{V_{22}} e^{2\gamma l}$$

Eqs. (A8) and (A9) simplify to

$$\begin{aligned} V_2 &= V_{22} e^{-\gamma z} (1 + \rho_2 e^{2\gamma(z-l)}) \\ I_2 &= \frac{V_{22}}{Z_0} e^{-\gamma z} (1 - \rho_2 e^{2\gamma(z-l)}) \end{aligned} \quad z' < z < l \quad (A10)$$

At  $z = z'$  the voltage must be continuous. This implies that  $V_2(z') - V_1(z') = 0$ ; therefore,

$$e^{-\gamma z'} (1 + \rho_2 e^{2\gamma(z'-l)}) V_{22} - e^{\gamma z'} (1 + \rho_1 e^{-2\gamma z'}) V_{11} = 0 \quad (A11)$$

Similarly, the unit current at  $z'$  must be equal to  $I_2(z') - I_1(z')$ ; therefore,

$$e^{-\gamma z'} (1 - \rho_2 e^{2\gamma(z'-l)}) V_{22} - e^{\gamma z'} (\rho_1 e^{-2\gamma z'} - 1) V_{11} = Z_0 \quad (A12)$$



Using Cramer's determinant rule, we have

$$V_{22} = \frac{Z_0 e^{\gamma z'} (1 + \rho_1 e^{-2\gamma z'})}{2(1 - \rho_1 \rho_2 e^{-2\gamma l})} \quad (A13)$$

$$V_{11} = \frac{Z_0 e^{-\gamma z'} (1 + \rho_2 e^{2\gamma(z'-l)})}{2(1 - \rho_1 \rho_2 e^{-2\gamma l})}$$

Substituting the above into the equations for  $V_1$  and  $V_2$ , we have the Green's function for an arbitrarily terminated transmission line excited by a point current source at  $z'$ :

$$G(z, z') = \begin{cases} \frac{Z_0 (1 + \rho_1 e^{-2\gamma z'})}{2(1 - \rho_1 \rho_2 e^{-2\gamma l})} [e^{-\gamma(z-z')} + \rho_2 e^{\gamma(z+z'-2l)}] & z' < z < l \\ \frac{Z_0 (1 + \rho_2 e^{2\gamma(z'-l)})}{2(1 - \rho_1 \rho_2 e^{-2\gamma l})} [e^{\gamma(z-z')} + \rho_1 e^{-\gamma(z+z')}] & 0 < z < z' \end{cases} \quad (A14)$$

For our case where the current source is a travelling-wave, extending from  $z' = z_1$  to  $z' = z_2$ , and where the line is impedance-matched to  $z = 0$  and at  $z = l$  (see Fig. A1), Eq. (A14) reduces to

$$G(z, z') = \begin{cases} \frac{z_0}{2} e^{-\gamma(z-z')} & , z' < z \\ \frac{z_0}{2} e^{\gamma(z-z')} & , z < z' \end{cases} \quad (A15)$$

Using Eqs. (A3) and (A15) we have

$$V(z) = \frac{z_0 J'}{2} \begin{cases} \frac{e^{\gamma z}}{\gamma + i\beta'} \left[ e^{-(\gamma + i\beta')z_1} - e^{-(\gamma + i\beta')z_2} \right] & , 0 < z < z_1 \\ \frac{1}{\gamma - i\beta'} \left( e^{(\gamma - i\beta')z} - e^{(\gamma - i\beta')z_1} \right) + \frac{e^{\gamma z}}{\gamma + i\beta'} \left( e^{-(\gamma + i\beta')z_1} - e^{-(\gamma + i\beta')z_2} \right) & , z_1 < z < z_2 \\ \frac{e^{-\gamma z}}{(\gamma - i\beta')} \left( e^{(\gamma - i\beta')z_2} - e^{(\gamma - i\beta')z_1} \right) & , z_2 < z < l \end{cases} \quad (A16)$$

## APPENDIX B. WAVEGUIDE MODEL

The differential equation relating the electric field amplitude  $A$  to the driving current source  $J$  is

$$\frac{d^2 A}{dz^2} - \gamma^2 A = i\omega\mu \int_{-\frac{s}{2}}^{\frac{s}{2}} J\phi(x) dx \quad (B1)$$

It should be clear that, with some minor modifications, the transmission line results of Appendix A are applicable here since the two governing differential equations are similar. To see the effect of the waveguide shape and dimensions, however, we will derive the Green's function for Eq. (B1) independently of the transmission line results.

The Green's function  $G(z, z')$  satisfies

$$\frac{d^2 G}{dz^2} - \gamma^2 G = -\delta(z - z') \quad (B2)$$

and the excited field amplitude due to an arbitrary  $J(z)$  is then given by

$$A(z) = K \int_{z_1}^{z_2} J(z') G(z, z') dz' \quad (B3)$$

where  $K \equiv i\omega\mu \int_{-s/2}^{s/2} \phi(x) dx$  and  $z_1 < z < z_2$  is the extent of the current source  $J(z)$ . Referring to Fig. A1 and following the procedures of Appendix A, we define

$$G(z, z') = \begin{cases} A_1(z, z') & \text{for } 0 < z < z' \\ A_2(z, z') & \text{for } z' < z < l \end{cases} \quad (B4)$$

The solution of Eq. (B3) for  $0 < z < z'$  is

$$A_1 = A_{11} e^{\gamma z} + A_{12} e^{-\gamma z} \quad (B5)$$

where  $A_{11}e^{\gamma z}$  and  $A_{12}e^{-\gamma z}$  are the left and right propagating electric field amplitudes, respectively. From  $\vec{E} = A(z)\phi(x)\hat{y}$  and the Maxwell equation

$$H_x = \frac{\partial A}{\partial z} \frac{\phi(x)}{i\omega\mu} \quad (B6)$$

we obtain

$$H_x = \frac{A_{11}}{i\omega\mu} \left( e^{\gamma z} - \rho_1 e^{-\gamma z} \right) \phi(x) \quad (B7)$$

where  $\rho_1 = A_{12}/A_{11}$  is the amplitude reflection coefficient at  $z = 0$  given by

$$\rho_1 = \frac{Z_1 - Z_0}{Z_1 + Z_0} \quad (B8)$$

The field expressions in the region  $0 < z < z'$  are then given by

$$E_y = A_1 \phi = A_{11} e^{\gamma z} (1 + \rho_1 e^{-2\gamma z}) \phi(x) \quad (B9)$$

$$H_x = \frac{1}{i\omega\mu} \frac{\partial A}{\partial z} \phi = \frac{A_{11}}{Z_0} e^{\gamma z} (1 - \rho_1 e^{-2\gamma z}) \phi(x)$$

with  $Z_0 \equiv i\omega\mu/\gamma$  and  $A_{11}$  to be determined from the source conditions at  $z = z'$ .

Similarly, the field amplitude for  $z' < z < l$  is

$$A_2 = A_{22} (e^{-\gamma z} + \rho_2 e^{\gamma z} e^{-2\gamma l}) \quad (B10)$$

and

$$H_x = -\frac{A_{22}}{Z_0} (e^{-\gamma z} - \rho_2 e^{\gamma z} e^{-2\gamma l}) \phi(x) \quad (B11)$$

where  $\rho_2 = V_{21}/V_{22} e^{2\gamma l}$  is the reflection coefficient at  $z = l$ . The field expressions for  $z' \leq z \leq l$  are then given by

$$E_y = A_2 \phi(x) = A_{22} e^{-\gamma z} (1 + \rho_2 e^{\gamma z(z-l)}) \phi(x) \quad (B12)$$

$$H_x = \frac{\partial A_2}{\partial z} \frac{\phi(x)}{i\omega\mu} = -\frac{A_{22}}{Z_0} e^{-\gamma z} (1 - \rho_2 e^{2\gamma(z-l)}) \phi(x)$$

At  $z = z'$ ,  $E_y$  must be continuous and so

$$e^{-\gamma z'} (1 + \rho_2 e^{2\gamma(z'-l)}) A_{22} = e^{\gamma z'} (1 + \rho_1 e^{-2\gamma z'}) A_{11} \quad (B13)$$

Now the magnetic field  $H_x$  at  $z'$  must be discontinuous to account for the point current source there. Quantitatively, from Eq. (B2) we have

$$\frac{d}{dz} A_2(z') - \frac{d}{dz} A_1(z') = -1 \quad (B14)$$

and so

$$e^{-\gamma z'} (1 - \rho_2 e^{2\gamma(z'-l)}) A_{22} + e^{\gamma z'} (1 - \rho_1 e^{-2\gamma z'}) A_{11} = Z_0 \quad (B15)$$

Since these equations are similar to those for the transmission line case in Appendix A, the procedures for finding the Green's function are identical and therefore will not be repeated here.

# APPENDIX C. WAVEVECTOR ERROR DUE TO MISALIGNMENT ERRORS

Let  $z$  be the true direction of propagation along the waveguide axis for the perfect phase-match case, and  $z'$  be the perturbed direction. We see from Fig. C1 that the alignment between the two lasers is described by the angle  $\theta$ , and that the laser misalignment with respect to the  $z$  axis (waveguide axis) is described by  $\phi_1$  and  $\phi_2$ . Let  $\hat{\beta}z$  be the wavevector of the dominant mode to be phase matched by the induced current source. Ideally, we would like to have

$$k_1 - k_2 = \hat{\beta}z \quad (C1)$$

Since  $|k_1| = |k_2| \equiv k$  for the frequency considered, we have

$$|k_1 - k_2| = 2k \sin \theta/2 \quad (C2)$$

We see from Eqs. (C1) and (C2) that the conditions for perfect phase-match are

$$2k \sin \theta/2 = \beta \quad (C3)$$

and

$$\frac{k_1 - k_2}{|k_1 - k_2|} = \hat{z}$$

For angle error  $\delta\theta \ll \theta$ ,

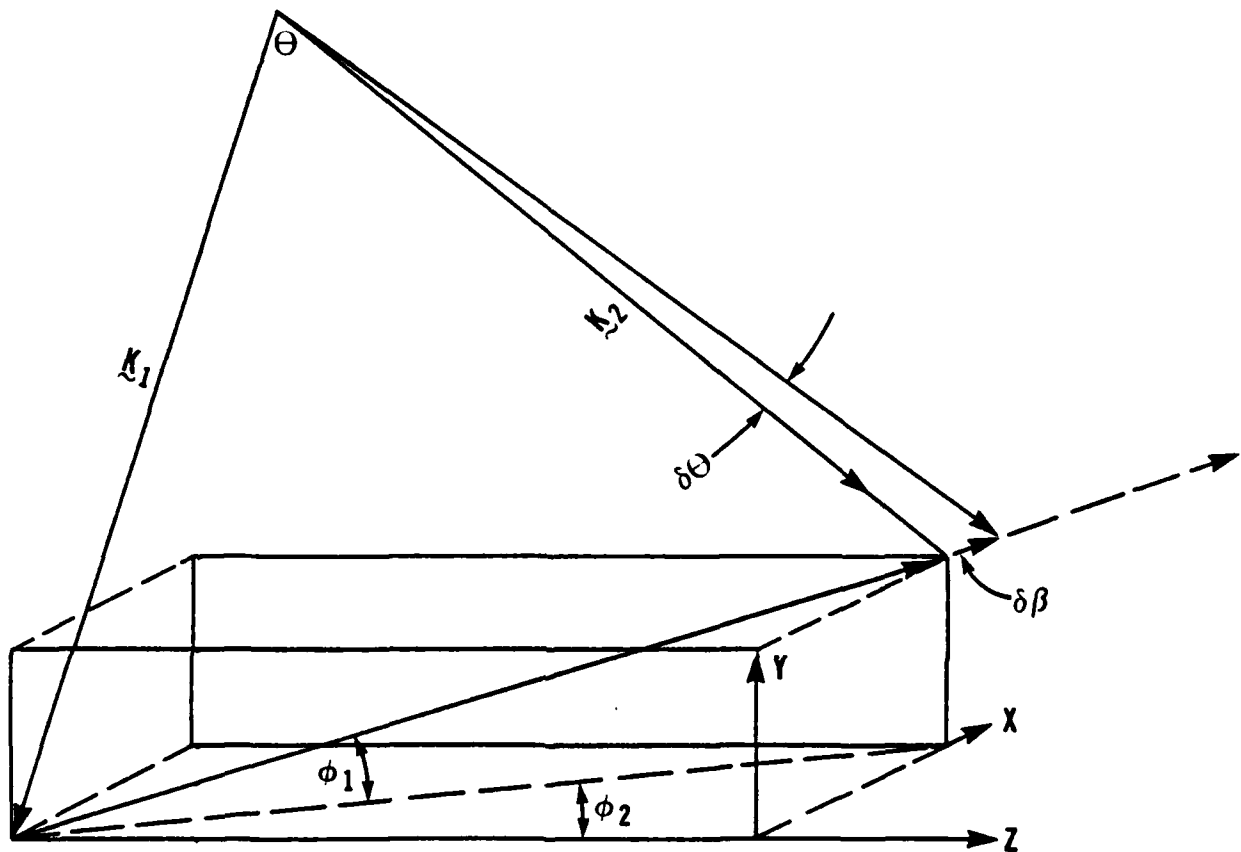


Figure C-1. Diagram of Wave Vector Mismatch Due to Laser Misalignment



$$|k_1 - k_2| = 2k \sin \frac{\theta}{2} + k \cos \frac{\theta}{2} \delta\theta = \beta + \delta\beta \quad (C4)$$

and the corresponding z component  $\beta'$  is then given by

$$\beta' = [2k \sin \frac{\theta}{2} + k \cos(\frac{\theta}{2}) \delta\theta] \cos \phi_1 \cos \phi_2 \quad (C5)$$

The overall wavevector mismatch ( $\delta\beta$ ) resulting from the misalignment angle,  $\delta\theta$ , and the orientation angles,  $\phi_1$  and  $\phi_2$ , is then given by

$$\delta\beta = \beta - \beta' = \beta \left( 1 - \cos \phi_2 \cos \phi_1 \left( 1 + \frac{\delta\theta}{\theta} \right) \right) \quad (C6)$$

## 6.0 REFERENCES

1. J. SooHoo, J. E. Miller, S. K. Yao, R. R. Shurtz II, R. A. Gudmundsen, and E. H. Huffman, "Generation of Millimeter Waves Utilizing a Laser-Induced Traveling-Wave Current," Digest of the Fifth International Conference on Infrared and Millimeter Waves, University of Wurzburg, Germany, Oct. 1980.
2. J. SooHoo, S. K. Yao, J. E. Miller, R. Shurtz, Y. Taur and R. A. Gudmundsen, "A Laser-Induced Traveling-Wave Device for Generating Millimeter Waves," IEEE Transaction on Microwave Theory and Techniques, Nov. 1981.
3. S. M. Sze, Physics of Semiconductor Devices, John Wiley and Sons, Chapter 5, New York (1977).
4. S. M. Sze and R. M. Ryker, "Microwave Avalanche Diodes," Proceedings IEEE, Vol. 59, p. 1140-1154, Aug. 1971.
5. P. J. Meier, "Integrated Fin-Line Millimeter Components," IEEE Trans. Microwave Theory Tech, Vol. MTT-22, p. 1209-1216, Dec. 1974.
6. S. Hopfer, "The Design of Ridged Waveguide," IEEE Trans. Microwave Theory Tech., Vol. MTT-3, p. 20-29, Oct. 1955.
7. W. J. Gettsinger, "Ridge Waveguide Field Description and Application to Directional Couplers," IEEE Trans. Microwave Theory Tech., Vol. MTT-10, p. 41-50, Jan. 1962.
8. S. B. Cohn, "Properties of Ridge Waveguide," Proceedings IRE Vol. 35, p. 783-788, Aug. 1947.
9. M. Franz and J. B. Beyer, "The Travelling-Wave IMPATT Mode," IEEE Trans. Microwave Theory Tech, Vol. MTT-26, p. 861-865, Nov. 1978.
10. Y. Taur, D. T. Cheung, E. H. Huffman, J. SooHoo, and R. A. Gudmundsen, "MM-Wave Generation at 110 GHz by Laser Modulation of a HgCdTe Photodiode," Vol. 38, No. 10, 819-821, May 1981.
11. C. C. Wang, M. Chu, S. H. Shin, W. E. Tennant, J. T. Cheung, M. Lanir, A.H.B. Vanderwyck, G. M. Williams, L. O. Bubulac, and R. J. Eisel, IEEE Trans. Elec. Dev., ED-27, 154 (1980).
12. L. O. Bubulac, W. E. Tennant, S. H. Shin, C. C. Wang, M. Lanir, E. R. Gertner, and E. D. Marshall, Japanese J. Appl. Phys., 19-1, 495 (1980).
13. E. R. Gertner and E. D. Marshall, Jpn. J. Appl. Phys. 19-1, 495 (1980).
14. A. R. Kerr, IEEE Trans. Microwave Theory and Tech. MTT-23, 781 (1975).



REFERENCES (CONTINUED)

15. T. A. Medford and H. C. Bowers, "A Two-Port IMPATT Diode Traveling Wave Amplifier," Proc. IEEE, Oct. 1968.
16. N. S. Navydova, Yu Z. Danyushensky and L. I. Telyatnikov, "Linear Theory of an IMPATT Diode Distributed Microwave Amplifier," Telecommun. and Radio Engr., Pt. 2, Vol. 27, No. 8, pp. 112-115, Aug. 1972.
17. K. G. Hambleton and P. N. Robson, "Design Considerations for Resonant Traveling Wave IMPATT Oscillators," Int. J. Electron., Vol. 35, No. 2, pp. 225-244, 1973.
18. W. T. Read, "A Proposed High-Frequency Negative Resistance Diode," Bell Syst. Tech. J., Vol. 37, March 1958, pp. 401-446.